Changes in effective stress during the 2003-2004 Ubaye seismic swarm, France

Running title: *Changes in effective stress during the Ubaye swarm*

G. Daniel[1], E. Prono[2], F. Renard[3,4], F. Thouvenot[5], S. Hainzl[6], D. Marsan[2], A. Helmstetter[5], P. Traversa[5], J.L. Got[2], L. Jenatton[5], and R. Guiguet[5]

[1] CNRS-Université de Franche-Comté, UMR 6249 Chrono-environnement, 16 route de Gray, 25030 Besançon, France

[2] Université de Savoie, LGIT-CNRS-Observatoire de Grenoble, 73376 Le Bourget du Lac, France

[3] Université Joseph Fourier-Grenoble I, LGCA-CNRS-Observatoire de Grenoble, BP 53, 38041 Grenoble, France

[4] Physics of Geological Processes, University of Oslo, Norway

[5] Université Joseph Fourier-Grenoble I, LGIT-CNRS-Observatoire de Grenoble, BP 53, 38041 Grenoble, France

[6] Institute of Geosciences, University of Potsdam, POB 60 15 53, D-14415, Potsdam, Germany

Abstract

We study changes in effective stress (normal stress minus pore pressure) that occurred in the French Alps during the 2003-2004 Ubaye earthquake swarm. Two complementary datasets are used. Firstly, a set of 974 relocated events allows us to finely characterize the shape of the seismogenic area and the spatial migration of seismicity during the crisis. Relocations are performed by a double-difference algorithm. We compute difference in travel-times at stations both from absolute picking times, and from cross-correlation delays of multiplets. The resulting catalogue reveals a swarm alignment along a single planar structure striking N130°E, and dipping 80°W. This relocated activity displays migration properties consistent with a triggering by a diffusive fluid overpressure front. This observation argues in favor of a deep-seated fluid circulation, responsible for a significant part of the seismic activity in Ubaye. Secondly, we analyze time series of earthquake detections at a single seismological station, located just above the swarm. This time series forms a dense chronicle of +16,000 events. We use it to estimate the history of effective stress changes during this sequence. For this purpose, we model the rate of events by a stochastic Epidemic-Type Aftershock Sequence model (ETAS) with a non-stationary background seismic rate $\lambda_0(t)$. This background rate is estimated in discrete time windows. Windows lengths are optimally determined according to a new change-point method, based on the inter-event times distribution. We propose that background events are directly triggered by a transient fluid circulation at depth. Then, using rate-and-state constitutive friction laws, we estimate changes in effective stress for the observed rate of background events. We assume that changes in effective stress occurred under constant shear stressing rate conditions. We

finally obtain a maximum change in effective stress close to -8 MPa, which corresponds to a maximum fluid overpressure of about 8 MPa under constant normal stress conditions. This estimate is in good agreement with values obtained from numerical modeling of fluid flow at depth, or with direct measurements reported from fluid injection experiments.

Keywords: ***Ubaye seismic swarm, Seismicity rate, Pore-pressure changes, Declustering, Rate-and-State laws, Earthquake relocations.***

1. Introduction

Seismic swarms are dense and intensive episodes of microseismic activity. Generally, they do not consist in a simple succession of many larger shocks and their aftershocks. They rather exhibit a complex behavior, compared to typical seismic crisis, initiating with an increasing number of small events and ending after a variable term. The study of these phenomena is thus very challenging, as they question the very detailed behavior of seismicity. Seismic swarms also reflect transient changes of in-situ physical properties in the upper crust. Consequently, the analysis of swarm episodes is of importance, as it may potentially bear crucial information on the general earthquake preparation process at a human time scale.

This study focuses on the Ubaye valley area (Alpes-de-Haute-Provence, France; see Figure 1), which is the most seismically active region in the French western Alps [*Thouvenot and Fréchet*, *2006*]. Seismic activity in this area is characterized both by moderate earthquakes (e.g. the historical M 5.5 Saint-Paul-sur-Ubaye earthquake in 1959) and episodic swarms. Using a temporary seismological network, *Fréchet and Pavoni (1979)* conducted the first study of a swarm in Ubaye. Subsequently, *Guyoton et al. (1990)* described another swarm episode in 1989, soon after the installation of the permanent seismological network Sismalp (http://sismalp.obs.ujf-grenoble.fr/). They located it 5 km NE of Saint-Paul. In the present study, we analyze the most recent swarm episode in this area, which started in January 2003 close to La Condamine-Châtelard, see Figure 1. This swarm consisted in a period of continuous seismic activity that lasted about two years. This sequence thus represents a new opportunity to improve our knowledge on the mechanics of swarm generation, and to study active faults in the Ubaye area.

In the literature, swarm occurrence is commonly related to the circulation of deep-seated fluids along, or in the vicinity of earthquake faults. Aseismic creep can also constitute an alternative trigger mechanism [*Lohman and McGuire, 2007*]. The close association between fluids and swarm relies either on direct observations of surface fluid flow accompanying the seismic activity (e.g. during the 1965-1967 Matsushiro swarm, Japan [*Tsuneishi and Nakamura, 1970*]), or on the close association of swarm episodes with areas of important gas outflow (e.g. the western Eger rift, Bohemia, Czech Republic [*Weinlich et al., 1999; Hainzl and Ogata, 2005; Bräuer et al, 2009*], the central Apennines, Italy [*Chiodini et al., 2000*]). Frequently, swarms occur in regions of geothermal or volcanic activity (e.g. swarms in the Long Valley caldera, California [*Savage et al., 1984; Hill and Prejean, 2005*]; at the Yellowstone volcanic field, western U.S. [*Farrell et al., 2009*]; or east of the Izu Peninsula, Japan [*Ukawa and Tsukahara, 1996*]). These peculiar settings suggest that stress perturbations associated with fluid overpressure at depth is a plausible mechanism for the driving of seismic swarms [e.g. *Yamashita, 1999; Hainzl and Ogata, 2005*].

During the Ubaye swarm, no fluid outflow was observed at the surface. However, the location of several hot springs located few tens of kilometers northwards and southwards from the study area reveals that current fluid circulations take place within the bedrock (Figure 1). According to these regional settings and to previous studies of swarms worldwide, we show here that a triggering of the Ubaye swarm by fluid overpressure is a very likely hypothesis. This hypothesis provides a coherent framework to explain the seismological observations. In section 2, we present the dataset elaborated for the Ubaye seismic swarm. We describe the spatio-temporal evolution of the relocated dataset in section 3, and present the characteristics of a diffusive migration pattern. In section 4 we model the rate of events and introduce a new

objective statistical procedure to estimate the non-stationary background-forcing rate in discrete time-windows. In section 5 we estimate the amplitude of the effective stress changes leading to the observed earthquake rate, deduced from the rate-and-state constitutive laws [*Dieterich, 1994*]. We finally discuss our results in section 6.

2. Data

This study relies on the analysis of two complementary seismological datasets. The first one is a relocated catalogue of micro-earthquakes, with magnitudes ranging between -0.3 and 2.7. This dataset was originally located by the Sismalp seismological network [*Thouvenot et al., 1990*]. The second dataset consists in a report of (hand-picked) event detections at JAUF, the closest seismological station (Figure 1). This station was located right above the earthquake swarm and allowed the detection of a large number of small events. This report constitutes a chronicle of 16,147 detections with M_L estimates ranging from -1.3 to 2.7 [*Jenatton et al., 2007*].

2.1 Relocated catalogue

Less than 10% of the 16,147 microearthquakes that occurred in Ubaye during years 2003 and 2004 were detected by a sufficient number of stations to be located. We have reprocessed the catalogue of earthquake relocations originally presented in *Jenatton et al. (2007)*. For this purpose, we have included phase picks at 5 supplementary stations (deployed in the area from September 2003 to December 2004), and improved its accuracy by using travel-times estimated from the cross-correlation of similar events (multiplets). All manual phase picks and cross-correlation delays were merged in a double-difference algorithm using the

116 HYPODD software [*Waldhauser and Ellsworth, 2000*]. The main advantage of this relocation
117 technique is that it allows the whole set of events to be located in a single operation. It also
118 preserves the high accuracy of relative relocations within the multiplet.
119 We obtain one single large multiplet of 799 events with a mean coherence greater than or
120 equal to 90% on at least 3 stations. High-precision travel time delay measurements were
121 performed by pair-wise cross-correlation of the first 1.28 second of seismic waveforms in the
122 spectral domain.
123 The computation of relocation uncertainties by a Monte-Carlo analysis led to an average
124 location error of 100 m. The relocated catalogue thus consists in 1058 events that occurred
125 between years 1989 and 2004. Among these, 974 earthquakes occurred during the crisis in
126 2003-2004 and are displayed on Figure 2. We present a map view (Figure 2, top) and a cross-
127 section (Figure 2, bottom) of the swarm, with events coordinates projected along a plane trend
128 of azimuth N130°E and dip 80°W.

129 **2.2 Detection time series at station JAUF**

130 The permanent seismological station JAUF recorded 16,147 events that could be hand-picked.
131 Differences in P- and S-waves arrival times were analyzed to select only events occurring
132 within the swarm area. Unfortunately, most of them could not be located as they triggered too
133 few or no other stations. Event magnitudes were estimated from peak amplitudes of
134 seismograms and distances, according to a calibration based on located events of the sequence
135 *[Jenatton et al., 2007*]. Magnitudes of this time-series span from -1.3 up to 2.7, leading to a
136 total energy release equivalent to that of a magnitude 4 event. These authors also showed that
137 magnitudes are consistent with a Gutenberg-Richter law [*Gutenberg and Richter, 1956*] with
138 a b-value of 1.2 ± 0.03. The time-series contains 3546 events with magnitude greater than the

completeness threshold M_L=0.2. This threshold has been determined by visual inspection, based on the validity of Gutenberg-Richter law for higher magnitudes. We here use origin times at JAUF to calculate the swarm seismicity rate (Figure 3, grey line). For the sake of comparison, and in order to verify that both datasets present a similar temporal evolution, we displayed the rate of the 974 relocated earthquakes on Figure 3 (black curve).

3. Spatial evolution of the swarm

This section focuses on two main features of the relocated catalogue. First, it reveals a precise image of the fault zone geometry (section 3-1) and second, it suggests a peculiar temporal evolution of the seismic activity along this structure (section 3-2).

3-1. Geometry of the seismogenic structure

In map view (see Figure 2a), the Ubaye swarm appears as an elongated narrow cloud of micro-earthquakes. The seismicity is mainly located within a narrow 8 km-long and 1 km wide band. At depth, all events are located on a quasi-vertical structure. This, however, does not guarantee that the seismic activity occurred on a single fault. Such a cloud may as well be defined, for example, by events distributed along a dense network of numerous short faults with different orientations. We now aim at determining the fault zone structure associated with this swarm. We assume that micro-earthquakes are not randomly distributed within a volume but rather occur along planar faults/fractures. We then search for the preferential plane orientations, by a simple geometrical analysis of hypocenters spatial distribution.

We use the 3-point method (*Fehler et al. 1987*) to detect preferential planar alignments of hypocenters. This method relies on the distribution of plane orientations (strike, dip) obtained for each possible set of 3 events in the relocated catalogue (i.e. among 974 events). As the

161 orientation of planes defined by close events will have larger uncertainties because of locations
162 errors, we restricted our analysis to events separated by at least 100 m. We also used a
163 maximum separation distance of 10 km in order to remove events located far from the main
164 swarm cluster. We remove the influence of the cluster elongated shape by normalizing the
165 distribution of plane orientation with respect to 100 random location sets within a volume of
166 comparable dimensions. We consider as significant every orientation occurring more than 3.62
167 standard deviations above the corresponding level obtained with the random datasets. This
168 corresponds to a ratio of 1 chance in 10,000 that this preferential alignment be indicated by
169 random variations around the mean number of similar orientations in the random dataset
170 [*Fehler et al., 1987*]. The preferred plane then corresponds to the most frequent orientation
171 above this threshold. This method also allows linking each seismic event with its preferred
172 plane orientation, interpreted as the fracture plane on which this event most likely fell. For this
173 purpose, we count how many times each event contributes to a set of 3 events aligned along a
174 particular orientation. Events with the largest number of counts are those that occur along this
175 particular plane.
176 Orientations of preferential planes are presented on Figure 4. Polar histograms display the
177 number of relocated earthquakes associated with each strike (see Figure 4, left) and dip (see
178 Figure 4, right) orientation. They show a clear prominence for planes striking N130°E ±5° and
179 dipping 80°±5° to the west, according to the convention used in *Aki and Richards (1980)*. This
180 range of orientations is in good agreement with the general trend of relocated seismicity, and is
181 also close to the N145°E direction obtained by *Jenatton et al. (2007)* from the set of original
182 locations. Interestingly, we find no preferential orientation striking perpendicular to the cloud
183 elongation direction, dismissing any possible interplay of conjugate faults during this episode.

We also notice that no temporal pattern is discernible in the evolution of the preferred orientation. Rather, the whole range of orientations represented on Figure 4 is associated with events from the initiation to the ending of the swarm episode. All these observations clearly argue in favor of a single seismogenic discontinuity at depth striking NW-SE and dipping 80°W.

3-2. Migration of the swarm activity

The most striking feature of the Ubaye crisis is certainly its temporal evolution. This is highlighted on Figure 2 by a color-scaling of hypocenters depending on their date of occurrence. Relocated events exhibit a quasi-unilateral migration of micro-earthquakes from the NW to the SE, within a band located between 3 and 8 km at depth.

We here discuss the diffusive character of the Ubaye swarm migration. For this purpose, we measure the progressive spreading of the main swarm cluster during the sequence. For each time t, we compute the average distance R between all events that occurred at time $t_i<t$ and the first earthquake of the sequence (Figure 5). Several previous studies have already documented the evolution of this distance R for earthquake sequences [*Noir et al., 1997; Marsan et al., 1999; Marsan et al., 2000; Helmstetter et al., 2003b; Huc and Main, 2003*]. For various global or regional earthquake catalogues, these authors found that R increases slowly with time, according to $R(t) \propto t^H$ with H close to 0.1 or 0.2. *Helmstetter et al. (2003b)* also noticed that this H value may vary from one individual sequence to another, and depends on the methods used to measure R. Such a relationship reveals that if a stress diffusion mechanism takes place within the Earth's crust, it occurs slowly, and may be very weak [*Marsan et al., 2000; Huc and Main, 2003*].

206 Inspection of Figure 5 reveals that the seismic activity in Ubaye started to spread about 30 days
207 after the swarm initiation. The average distance R increases up to the end of 2004, mainly
208 along the preferential plane orientation, see also Figure 2. Interestingly, the spreading of the
209 Ubaye sequence exhibits a quasi-diffusive character, characterized by a diffusion exponent
210 value $H=0.41 \pm 0.06$. Thus, not only did this swarm migrate very clearly, but also this
211 migration took place according to a process closer to a normal diffusion (i.e. with $H=0.5$) than
212 to the sub-diffusive process expected for typical earthquake sequences.
213 Normal diffusion processes characterize particle motions in physical systems close to
214 equilibrium [e.g. *Vlahos et al., 2008*]. Within the Earth's crust, such behavior may either be
215 related to a viscous relaxation mechanism, or to a pore-pressure balancing mechanism induced
216 by fluid flow in a relatively homogeneous medium. In Ubaye, as the depth of relocated
217 hypocenters lies within the upper, elastic, brittle part of the crust, we rather support the latter
218 mechanism, i.e. fluids. We argue that a deep increase in pore-pressure by fluid flow is the most
219 likely mechanism, and could unclamp favorably oriented faults/fractures by decreasing the
220 effective normal stress. In other words, we claim that seismicity in Ubaye is the result of a non-
221 stationary forcing by fluids, a well-known likely mechanism for the generation of earthquakes
222 [e.g. *Nur and Booker, 1972*].
223 For several years hydraulic fracturing studies have been focusing on the relationship between
224 such temporal spreading of the micro-seismicity and physical properties of the fractured
225 medium, e.g. permeability [see *Shapiro et al. 1997, Shapiro et al., 2006b* for instance].
226 Although their approach appears very attractive to characterize the fracturing process taking
227 place during the swarm, these physical models require boundary conditions, or experimental
228 settings, quite unlikely for natural seismic swarms. For instance, a constant fluid injection rate

may not be adequate for the Ubaye swarm, in reference with the size of the seismogenic volume and the long duration (2 years) of this episode. Nonetheless, the planar shape of the hypocenters cloud reveals that a fault zone with a higher permeability than the surrounding host rock was preexisting in the basement. When fluids invaded the medium during the swarm episode, this zone thus provided a natural channel for fluid circulation, and consequently, for earthquake occurrence. Recently, *Shapiro and Dinske* (2009) proposed a generalized model for microearthquakes migration that involves a nonlinear diffusion of fluids. According to their results, $H \neq 0.5$ may either follow from a pressure-dependent diffusivity parameter, or from a time varying fluid injection rate. These two mechanisms may have likely controlled the migration process observed in Ubaye.

4. Non-stationary forcing of seismicity by fluids

The driving of seismic swarms by fluids has been reported as a likely mechanism in numerous studies [e.g. *Hill et al., 1977; Yamashita,1999; Horálek and Fischer, 2008*], although surface evidences of fluid flow are scarce [e.g. *Tsuneishi and Nakamura, 1970*]. Indeed in Ubaye no fluid outflow was observed during the sequence [*Jenatton et al., 2007*]. In the following, we hypothesize that a transient fluid circulation at depth led to a significant part of the swarm activity, the remaining part resulting from self-sustained cascades of aftershocks [*Hainzl and Ogata, 2005*]. We have developed a new methodology in order to retrieve the rate of micro-earthquakes induced by a non-stationary background forcing in discrete time-windows. We later associate this forcing with effective stress changes at depth. The procedure that we describe in the following aims at modeling the seismicity rate recorded at station JAUF as a stochastic process.

The earthquake rate detected at JAUF (Figure 3) cannot be consistent with a typical mainshock-aftershock sequence. In Ubaye, we could not model satisfactorily the sequence as a succession of aftershock sequences obeying the Omori law superimposed on a Poissonian background rate. Such a behavior would lead to a temporal seismic response similar to that modeled with an Epidemic-Type Aftershock Sequence model (ETAS) with a constant background seismicity term [*Kagan and Knopoff, 1987; Ogata, 1988*]. Conversely, suitable modeling of this sequence requires the involvement of a non-stationary background rate. Consequently, we model the earthquake timeseries in Ubaye by a time-dependent Poisson process. The probability to observe *k* seismic events during a time interval *dt* is given by

$$P(k \mid \Lambda) = e^{-\Lambda} \frac{\Lambda^{-k}}{k!} \tag{1}$$

where $\Lambda = \int_{t-dt}^{t} \lambda(s)\, ds$

The rate $\lambda(t)$ consists in the superposition of two distinct contributions: a non-stationary background term $\lambda_0(t)$ and an epidemic term $\lambda_e(t)$. This last term explicitly stands for the probability that each event of the sequence generates its own secondary aftershocks [*Kagan and Knopoff, 1987; Ogata, 1988*],

$$\lambda(t) = \lambda_0(t) + \lambda_e(t) \tag{2}$$

with

$$\lambda_e(t) = \sum_{i;t_i<t} \frac{A e^{\alpha(M_i - M_C)}}{(t - t_i + c)^p} \tag{3}$$

In this expression, t_i and M_i are, respectively the occurrence time and magnitude of an earthquake *i*, whose magnitude is greater than, or equal to the magnitude of completeness M_c. A, α, c and p are epidemic parameters. This formulation has been used in previous studies to model seismicity rates and to retrieve the evolution of the non-stationary rate. Related studies

by *Hainzl and Ogata (2005)* applied such modeling to the Vogtland-West Bohemia swarm, and *Mastsu'ura and Karakama (2005)* to the Matsushiro swarm, Japan. Both studies improved significantly the modeling of seismicity rates with respect to an ETAS model with a constant background term $\lambda_0(t)$. In addition, *Hainzl and Kraft (2006)* related this non-stationary forcing $\lambda_0(t)$ to changes in pore pressure P according to the formula

$$\lambda_0(t) = \lambda_{00} + K\frac{\partial P}{\partial t} \qquad (4)$$

where λ_{00} is a constant background rate and K is a proportionality constant. This link was recently confirmed by *Llenos et al. (2009),* who showed that, during swarm episodes, aseismic forcing (e.g. fluids or creep) influences preferentially the background activity rate rather than other epidemic parameters of the ETAS model.

Model estimation is here performed in two steps. Firstly, we determine an optimal set of discrete time windows and estimate their respective background rate $\lambda_0(t)$ for each time window, based on the distribution of earthquake inter-event times. Secondly, we obtain the 4 epidemic parameters (A, α, c and p) that best explain the observed seismicity rate, using a maximum likelihood procedure.

4-1 Discretization of $\lambda_0(t)$

Objective discretization of the function $\lambda_0(t)$ is an important concern. Indeed, there exists a tradeoff between a choice of long time windows - that preserve the epidemic character of the model but prevent to retrieve rapid changes of the forcing rate, - and a choice of short time windows that tend to annihilate the epidemic contribution $\lambda_e(t)$. In the first situation, the model converges towards the original ETAS formulation [*Ogata, 1988*] as the length of time windows tends towards the length of the sequence. In the last situation, the model converges towards

294 $\lambda(t)=\lambda_0(t)$ as the length of time windows tends towards 0. In both cases, we may miss crucial
295 information concerning the interplay between a time-dependent external forcing $\lambda_0(t)$ and the
296 self-triggering $\lambda_e(t)$ of the seismic activity.
297 To overcome this difficulty, we here propose an objective procedure that optimizes the
298 discretization of the time axis into separate intervals for the estimation of $\lambda_0(t)$. We aim at
299 finding successive non-overlapping time windows during which we consider the background
300 external forcing $\lambda_0(t)$ as constant. The estimation of $\lambda_0(t)$ for each time window is based on the
301 method of *Hainzl et al. (2006)* that builds upon the fact that the probability density function of
302 inter-event times can be expressed as

303 $$f(\delta t) = C.e^{-a.\delta t}.(\delta t)^{-b} \quad (5)$$

304

305 with

306 $$C = \frac{a^{1-b}}{\Gamma(1-b)} \quad (6)$$

307 where δt are the inter-event times, C is a normalization constant and Γ is the gamma function.
308 *Hainzl et al. (2006)* showed that a and b can be estimated by

309 $$a = \frac{\overline{\delta t}}{\sigma^2_{\delta t}} \quad (7)$$

310 $$b = 1-(\overline{\delta t}.a) = 1-\frac{\overline{\delta t}^2}{\sigma^2_{\delta t}} \quad (8)$$

311 We note that this approach relies on the hypothesis of independent inter-event times, and that
312 taking into account their interdependence may affect our results. Following these authors, we

thus estimate the background rate as $\lambda_0(t)=a$. To evaluate the quality of the model $f(\tau)$, we divide the δt-axis into N bins $]0, \delta t_1],]\delta t_1, \delta t_2], \ldots$ such that $\{\delta t_1, \delta t_2, \ldots, \delta t_N\}$ are the observed inter-event times ranked in ascending order. For a given bin $]\delta t_{i-1}, \delta t_i]$ we observe exactly one occurrence (δt_i) of the inter-event times, while the model predicts

$$\mu_i = N \int_{\delta t_{i-1}}^{\delta t_i} d\delta t . f(\delta t) \tag{9}$$

occurrences, on average. We thus define the likelihood $\ell = \prod_{i=1}^{N} e^{-\mu_i} . \mu_i$ of the model, or equivalently

$$L = -\log(\ell) = \sum_{i=1}^{N} \mu_i - \ln(\mu_i) \tag{10}$$

Following the gamma law of *Hainzl et al. (2006)*, equations (9) and (10) can be written as

$$\mu_i = N.P(1-b, a.\delta t_i) - N.P(1-b, a.\delta t_{i-1}) \tag{11}$$

$$L = -\log(\ell) = N.P(1-b, a.\delta t_N) - \sum_{i=1}^{N} \ln(\mu_i) \tag{12}$$

where P is the lower incomplete gamma function.

In order to optimize the selection of time windows during which $\lambda_0(t)$ is modeled as constant, we use an objective change-point analysis. The rationale of the method is the following: let consider a time period with N inter-event times $\{\delta t_1, \delta t_2, \ldots, \delta t_N\}$. We want to know if this time period is better characterized by a change in λ_0 at a time t such that there are N_1 inter-event times for the time series prior to t and N_2 after t ($N=N_1+N_2$). We thus compare the two hypotheses:

- $\lambda_0(t)$ does not vary significantly between these two windows, hence a single model $f(\delta t)$ can well describe the inter-event time distribution for the time period ;

- $\lambda_0(t)$ varies significantly between these two windows, and we need to define two distinct densities f_1 and f_2, one for each window.

In the first case, the log-likelihood is L_1 as obtained from equation (12). In the second case, we compute L_2 from equations (9) and (12), but with

$$f(\delta t) = \frac{N_1}{N_1 + N_2} f_1(\delta t) + \frac{N_2}{N_1 + N_2} f_2(\delta t) \tag{13}$$

where f_1 and f_2 are parameterized independently for each window.

We search for the best time t (i.e. the change-point) by minimizing L_2. This change-point is then kept if L_2 is significantly lower than L_1. An objective procedure is to use the Bayesian Information Criterion [*Davison, 2003*]:

$$BIC = 2L + n\ln(N) \tag{14}$$

where n is the number of free parameters in the model ($n_1=2$ in the first hypothesis of only one density, $n_2=5$ in the second hypothesis of two densities and a change-point). We keep the change-point if $\Delta BIC=2*(L_2-L_1)+(n_2-n_1)*ln(N)$ is negative, hence $L_2-L_1<-3/2*ln(N)$.

This procedure starts with the entire window and is iterated until no further change-point is required. For the Ubaye swarm, we obtain a set of 6 discrete time windows for $\lambda_0(t)$ corresponding to the interval between two successive change-points. Figure 6 displays the fit of empirical inter-event times distributions by gamma distributions from equation 5. These diagrams show a good agreement between all inter-event times and the gamma law. By

estimating $\lambda_0(t)$ for each time interval associated with time windows defined according to this change-point method, we ultimately provide the stair-step estimate of $\lambda_0(t)$, see Figure 7 (dashed line) and Table 1.

4-2 Epidemic parameters estimate

We estimate the best set of epidemic parameters $\hat{\theta} = \{A, \alpha, c, p\}$ by a maximum likelihood procedure. We define it as the one that maximizes the following log-likelihood function:

$$L'(\theta) = \sum_k \ln \lambda(t_k; \lambda_0; \theta) - \int_0^T \lambda(t; \lambda_0; \theta)\, dt \qquad (15)$$

where T is the duration of the catalog, and t_k are earthquake occurrence times. We suppose parameters A, α, c and p to be constant, i.e. we make the hypothesis that the self-triggering process remains the same during the whole swarm sequence. Considering the seismicity rate model given in equations (2) and (3), we note that, for any θ, the log-likelihood value will depend strongly on the shape of $\lambda_0(t)$. As our strategy for the estimation of $\hat{\theta}$ relies on an independent estimate of $\lambda_0(t)$, this procedure guarantees a robust estimation of $\hat{\theta}$.

Again, we use the BIC criterion (equation 14) with n=4 (number of epidemic parameters), L=L' and N=3546 to check that the ETAS model with a non-stationary rate $\lambda_0(t)$ significantly improves the modeling, with respect to the formulation involving only a stationary background seismicity rate. The non-stationary parameterization leads to a BIC value of -10304, which is smaller than the value of -9880 obtained for the stationary background model. This decrease of the BIC criterion thus ensures that the non-stationary model provides a better fit to the data, while preserving a reasonable level of model complexity.

Best epidemic parameters correspond to values of A=0.0199 ± 0.0006, α=1.246 ± 0.014, c=(1.35 ± 0.67).10^{-4} and p=1.065 ± 0.001. Confidence intervals here correspond to the range of

values enclosing a 63% decrease of the likelihood function. Interestingly, these estimates of parameters A, α, c and p fall within the common range for seismicity observed in typical tectonic environments [*Ogata, 1992*]. This indicates that the self-triggering process in Ubaye is very similar to what is observed along major faults at plate boundaries [e.g. *Helmstetter et al., 2003a*; *Marsan and Lengline, 2008*]. We also interpret this close similarity as an indication that our modeling procedure properly succeeded at separating both contributions from, on one hand, the non-stationary forcing and on the other hand, the cascading process of secondary aftershocks.

The resulting model (black curve) of the swarm seismicity rate is in very good agreement with the rate observed at JAUF (gray curve), see Figure 7. This figure also displays the contribution of the non-stationary forcing rate $\lambda_0(t)$ (dashed curve) to the total seismicity rate of the Ubaye swarm. The forcing-induced activity rate increases progressively from the beginning of the swarm up to its apex between day 174 (2003/06/23) and day 350 (2003/12/16), when it led to about 5 events per day. Afterwards, this forcing slowly and progressively weakens towards the end of 2004. The general evolution of the forcing rate consequently presents an evolution that is quite similar to the overall trend of observed activity. This is an indication that low frequency variations of the earthquake rate may be related to a slow and progressive external forcing mechanism, while high frequency variations may be related to cascades of aftershocks sequences. We also note that our model fails at reproducing the amplitude of the four prominent peaks of seismic activity occurring respectively at days 174, 198, 243 and 276. This failure is a direct consequence of the definition of $\lambda_0(t)$ as a stair-step function. Indeed, by keeping a constant value for $\lambda_0(t)$ in each time window, we prevent the model to adapt rapid

395 fluctuations of the background-forcing rate, probably related with strong transients of the fluid
396 overpressure.
397 As explained in the previous section, our estimates of the background rate rely on *Hainzl et al*
398 *(2006)*'s method. In Table 1 we also provide estimates obtained from two other procedures.
399 The first alternative technique consists in inverting jointly the ETAS epidemic parameters and
400 background values for all windows (we use time windows as presented in Figure 7). The
401 second alternative technique attempted at reconstructing the background rate from the
402 difference between the observed rate of event and the rate of triggered events (estimated from
403 the ETAS triggering kernel using A, α, c and p estimates presented in this section). This daily
404 background rate estimate was initially smoothed over a 100 days time window, and afterwards
405 averaged for each of the time windows defined above. Although the joint inversion technique
406 delivers background rate values quite close to estimates using *Hainzl et al (2006)*'s method, the
407 second alternative "background reconstruction" technique show higher discrepancies in respect
408 to this method. Such differences between background rate estimates for these two techniques
409 (see Table 1) may partly be due to the smoothing used for the background reconstruction
410 technique (alternative 2), and to the use of different sets of parameters A, α, c, and p. However,
411 all of background rate estimation techniques explained here present overall a reasonable level
412 of coherency, and background rate estimates undergo very similar evolution patterns.

413 For the next part of the analysis, we use the background estimates obtained using the modified
414 change-point procedure described in section 4-1. This technique presents the advantages of
415 being the most objective, and the most appropriate method to decluster the Ubaye dataset.
416 Alternative modeling using time windows with constant duration, or constant number of events

417 have proved to lead to worse adjustments, in terms of BIC values. Best results have been
418 obtained using the modified change-point technique.

419

420 5. Retrieval of effective stress changes

421 In this section, we estimate changes in effective stress (normal stress minus pore pressure)
422 using the earthquake rate at JAUF declustered from its epidemic cascades of aftershocks. The
423 link between the seismicity rate and stress changes arises from the constitutive laws based on
424 rate-and-state friction and proposed by *Dieterich (1994)*.
425 In the following, we hypothesize that the rate $\lambda_0(t)$ is directly related to a time-dependent
426 change in effective stress within the swarm area. According to the Mohr-Coulomb criterion a
427 decrease of the effective stress $\sigma = \sigma_n - \tilde{p}$ may favor the friction of rocks (i.e. earthquake
428 occurrence) by unclamping faults at depth. Such a decrease of the effective stress can either be
429 related to a decrease in normal stress σ_n, or to an increase in pore-pressure $\tilde{p}$. This also
430 amounts to consider that cascades of secondary aftershocks ($\lambda(t)-\lambda_0(t)$) reflect the amount of
431 seismicity triggered by shear stress changes on optimally oriented fault planes.
432 *Dieterich et al. (2000)* showed that local Coulomb stress changes could be estimated from the
433 temporal changes of the seismicity rate in a given region. According to these authors, there is a
434 non-linear relationship between stress changes and seismicity rates for a population of faults
435 governed by rate-and-state friction laws [*Dieterich, 1994*]. The seismicity rate R depends on a
436 state variable γaccording to

437
$$R = \frac{r}{\gamma \dot{\tau}_r} \qquad (16)$$

438 where r is a reference seismicity rate under a reference shear stressing rate $\dot{\tau}_r$. The evolution of
439 the state variable γ is governed by the following differential equation:

440 $$d\gamma = \frac{1}{A'\sigma}\left| dt - \gamma d\tau + \gamma\left(\frac{\tau}{\sigma} - k\right)d\sigma \right| \quad (17)$$

441 In this expression, A' and k are constitutive parameters, σ stands for effective stress and τ for
442 shear stress.

443 Here, we set $R(t)=\lambda_0(t)$, and we calculate $\gamma(t)$ by use of equation 16. We use a quasi-static
444 formulation of equation 17 with time steps of length dt=1 day. For each time step, $\sigma(t+dt)$
445 corresponds to $\sigma(t)+d\sigma$, where $d\sigma$ is obtained by solving equation 17. In other words, we
446 assume a constant stressing rate for shear stress ($d\tau = \dot{\tau}\, dt$) and a quasi-static evolution of
447 effective stress $d\sigma$ and γ, with $d\gamma=\gamma(t+dt)-\gamma(t)$. This approach tends to underestimate large
448 amplitude, short-lived changes in $|d\sigma|$ as the background rate is averaged over longer time
449 intervals (see the discussion on time windows in section 4-1).

450 We select parameters values according to values reported in the literature. We consider a
451 secular linear increase in shear stress with time of $\dot{\tau}$ =2.5 kPa.yr^{-1}, based on geodetic estimates
452 in the area [*Ferhat et al., 1998*] and on a shear modulus equal to $0.25 \cdot 10^{11}$ Pa. This hypothesis
453 for shear stress changes appeared as the most reasonable due to the likely influence of fluid
454 pressure on the swarm activity. In addition, to the authors' knowledge, no complementary
455 geodetic dataset exists to better constrain the evolution of $d\tau$ during this episode. The
456 reference earthquake rate r for $M_L \geq 0$ is estimated from the rate r_1 of $M_L \geq 1$ event located in the
457 area between 1989 and 2002, when no prominent seismic activity occurred. We obtain r_1= 0.3
458 event/year with $M_L \geq 1$ from the relocated catalogue, which leads to $r = r_1 \cdot 10^{b(1-0.2)} = 2.74$
459 events/year with $M_L \geq 0.2$. We express changes in effective stress relatively to a reference

steady-state value σ_0 before the swarm initiation. We choose σ_0 to be equal to the overburden pressure (with bulk density $\rho=2700$ kg.m^{-3}) minus the hydrostatic pressure at 5 km depth. This leads to a steady-state effective stress of $\sigma_0=83$ MPa. According to equation 17 the amplitude of effective stress changes $d\sigma$ is directly related to σ_0. We have also observed that the relative height of stress steps increases when σ_0 increases. As a consequence, the selection of initial hydrostatic conditions thus represents a lower bound for changes in effective stress, that is, respectively, a higher bound for changes in pore-pressure. Initial shear stress was chosen to be equal to 0.6 times the steady-state effective stress, i.e. we suppose the crust to be close to a critical state for rupture. Laboratory measurements suggest that the A' parameter usually ranges between *0.005* and *0.015* [*Dieterich et al., 2000*]. As we have no a priori knowledge on pressure and temperature conditions within the source volume, we choose an average value, i.e. $A'=0.01$. The resulting amplitude of effective stress is also related to the value of parameter A', see equation 17, although stress changes remain of the same order. That is, we obtained maximum stress changes of *-3* and of *-9* MPa, respectively for A' equal to *0.005* and *0.015*. Parameter *k* is set equal to *0.23* [*Linker and Dieterich, 1992*].

Figure 8 displays the effective stress history obtained using this procedure. The step-like shape is obviously unrealistic but is directly inherited from assumptions on $\lambda_0(t)$. This curve should consequently be understood as a first-order estimate of effective stress changes during the swarm. Negative changes in effective stress mean that the triggering of micro-earthquakes during the Ubaye swarm occurred either by a decrease in normal stress or by an increase in pore-fluid pressure. Finally, if one assumes constant normal stress conditions, this result suggests that a pore-pressure increase of about 8 MPa was sufficient to generate 41% (1448

482 background events) of the seismic activity in Ubaye between January 2003 and December
483 2004.

484 6. Discussion

485 In the previous sections, we have shown that the Ubaye swarm *i)* occurred on a simple planar
486 structure striking N130E and dipping 80°W, *ii)* exhibited an unusual diffusive migration of
487 hypocenters towards the SE, and *iii)* required the contribution of an external non-stationary
488 forcing rate in addition to the self-triggering of seismicity (via cascades of secondary
489 aftershocks). Assuming that fluid circulations at depth induced a significant part of this
490 activity, we explain the migration of earthquake hypocenters as the result of a fluid diffusion
491 process within the crystalline basement. Moreover, the distribution of seismicity along a
492 preferential plane suggests that fluids may have propagated through a more permeable channel,
493 possibly inherited from a preexisting fault structure. The diffusive migration of hypocenters
494 during the swarm is also an indication that fluid overpressure at depth was not high enough to
495 open new fractures in the medium.
496 The evocation of deep fluid circulation is of common use for explaining the spatial and
497 temporal properties of seismic swarms [*Horálek and Fischer, 2008*]. In Ubaye, although no
498 fluid outflow was observed during the sequence, we propose that a fluid overpressure at depth
499 was responsible for the 2003-2004 swarm episode. First, this proposition relies on the
500 similarity of the earthquake migration pattern with those observed during other swarm episodes
501 that have been convincingly related with fluid circulations [*Tsuneishi and Nakamura, 1970;*
502 *Horálek and Fischer, 2008*]. Second, it also relies on considerations about the present and past
503 fluid circulations in the same bedrock, observed few kilometers further south. Recalling that
504 the swarm activity was confined within a 3 to 8 km band at depth, the seismogenic structure of

505 the swarm is most probably confined within the crystalline bedrock, rather than within the
506 overlying 1- to 2-km-thick Embrunais-Ubaye nappe [*Jenatton et al., 2007*]. The bedrock crops
507 out few kilometers south of the Ubaye valley, forming the Argentera Massif. In this massif,
508 numerous outcropping fault structures and rock weathering related with fluid circulations can
509 be studied directly in the field. Fault structures show preferential orientations along a direction
510 sub-parallel to the swarm alignment (see *Baietto et al., 2009* and references therein).
511 Furthermore, several places in the Argentera Massif are well known for their geothermal
512 activity, like Bagni di Vinadio, Italia, or Terme di Valdieri, Italia, about 15 km southeast of the
513 former (Figure 1). *Baietto et al. (2008; 2009)* studied the geological settings related with
514 geothermal circulations in these areas. They reported an important fluid outflow at Terme di
515 Valdieri, with a bulk discharge rate of 50 $kg.s^{-1}$ and a fluid temperature reaching up to 70°C.
516 According to these authors, fluids chemical properties are also consistent with a circulation
517 path within the crystalline basement, that is, going down to 5-6 km depth below the surface. As
518 a consequence, the involvement of fluid circulations within the basement in Ubaye appears a
519 very reasonable hypothesis, and is quite consistent with circulation depth estimated in the
520 Argentera area.
521 The analysis presented in section 5 shows that changes in effective stress can be estimated by
522 use of the complete form of the differential equation for rate-and-state constitutive laws (see
523 equation 17). Assuming constant normal stress during the sequence, a progressive increase in
524 pore-pressure up to about 8 MPa could be sufficient to trigger the *16,147* events swarm. Figure
525 8 also shows that pore-pressure progressively increased to this maximum value in 350 days,
526 and decreased afterwards by 7 MPa in about 350 days. This slow evolution of the pore-
527 pressure may explain the particularly long duration of this swarm episode.

These estimates of pore-pressure change are in good agreement with numerical modeling of fluid circulations during swarm episodes, and with observations from fluid injection experiments. In a recent study of the 1965-1967 Matsushiro swarm in Japan, *Cappa et al. (2009)* argued that pore-pressure changes of 4 MPa were necessary to quantitatively reproduce the observed seismicity, deformation, and fluid outflow at the surface. *Hainzl and Ogata (2005)* also found that a pore-fluid diffusion mechanism with a maximum pore-pressure change of 2 to 5 MPa was compatible with the seismic properties of the Vogtland-West Bohemia swarm. In another example, *Miller et al. (2004)* showed that CO_2 pore-pressure changes of about 10-20 MPa can explain the spatial migration of the 1997 sequence of 6 M>5 earthquakes in central Italy. These authors also argued that such changes in pore-pressure are large enough to overwhelm static shear stress changes. In Ubaye, we find that for pore-pressure changes of about 8 MPa, shear stress transfers (leading to successive cascades of aftershocks) could still induce 59% of the seismic activity. Our estimates also agree with the results of *Cornet et al. (1997)* who reported seismicity in response to overpressure between 5 and 10 MPa during the 1993 fluid injection experiment at Soultz-sous-Forêts, France. The initiation of the swarm activity for very slight pore pressure changes (< 1 MPa) during the first days of 2003 is also very consistent with the conclusions of *Zoback et al. (1997)* and *Shapiro et al. (2006a)*, and confirms the critical state of the fault before the swarm episode.

Toda et al. (2002) proposed that earthquake swarms might be driven by change in shear stressing rate. They proposed that, according to this principle, aftershock duration would decrease with increasing shear stressing rate changes. However, we show here that the decrease in effective stress due to pore-pressure diffusion at depth constitutes another viable explanation for swarm generation. Our results also indicate that the seismicity in Ubaye area results from

551 the superposition of a time-varying external forcing over cascades of seismicity with constant
552 aftershock duration.

553 7- Conclusion

554 We have presented a new analysis of the Ubaye seismic swarm. This study relies on the
555 catalogue built by the French Sismalp seismological network, which we improved by
556 relocating 974 earthquakes. We also used the time series of 16,147 event detections at station
557 JAUF in 2003-2004. We have identified a clear spatial migration of earthquakes, along a sub-
558 vertical N130E fault structure. We interpreted this as the result of fluid circulation at depth.
559 Thus, the initiation and development of the Ubaye swarm could be related to the diffusive
560 propagation of fluid overpressure within the crystalline basement. An important result of this
561 study is the assessment of the associated fluid overpressure from the analysis of the earthquake
562 rate. This calculation is based on rate-and-state constitutive laws applied to the non-stationary
563 rate of fluid-driven (i.e. background) seismicity. We found that pore-fluid pressure varied with
564 time during the swarm sequence, with a maximum excess of pore-pressure of 8 MPa, with
565 respect to the level that preexisted before January 2003. This value is comparable with
566 estimates from numerical modeling of swarms in Italy and in Japan, or with direct pressure
567 measurements realized during fluid injection experiments.
568 Besides, some aspects of the fracture process still remain open questions, and could not be
569 addressed within the framework of the present study. For example, was the permeable channel
570 localized within the core or within the damage zone of the source fault? What was the
571 physico-chemical nature of fluids involved? How can we model their path to the seismogenic
572 zone? Did the presence of the overlying nappes in Ubaye played a role in the structure design
573 of the source?

574 Each of these aspects needs further investigation in the framework of a careful geological
575 study of the area. Clarifying the process of fluid refill, its behavior at depth and its interplay
576 with the basement geology are now essential steps to consider for a comprehensive
577 explanation of episodic swarm occurrences in the Ubaye valley, and worldwide.

578 ## Acknowledgments

579 E.P. was supported by the CNRS-ANR ASEISMIC project. We also acknowledge the
580 following institutions for their support to the Sismalp permanent network. The conseil général
581 de l'Isère, the Délégation aux Risques Majeurs (French Ministry of the Environment), the
582 Institut National des Sciences de l'Univers (CNRS), and the Conseil Régional Rhône-Alpes
583 funded the Sismalp network. The Bureau Central Sismologique Français, the regional
584 direction of the Environment (Dreal Rhône-Alpes), the Observatoire de Grenoble (OSUG),
585 and the Conseils Généraux (Isère, Alpes-de-Haute-Provence, Hautes-Alpes, Haute-Savoie,
586 Ain, and Savoie) support its running costs. The authors would like to thank the associate
587 editor and two anonymous referees for their thorough reviews and helpful suggestions.

588 **References**

589 Aki, K., and Richards, P.G., 2002, Quantitative Seismology, 2nd Edition, University Science
590 Books, 704p.

591 Baietto A., P. Cadoppi, G. Martinotti, P. Perello, P. Perrochet, and F.-D. Vuataz (2008),
592 Assessment of thermal circulations in strike-slip fault systems: the Terme di Valdieri case
593 (Italian western Alps). *In:* Wibberley C.A.J., W. Kurz, J. Imber, R.E. Holdsworth, and C.
594 Colettini (Eds): The internal structure of fault zones: implications for mechanical and fluid-
595 flow properties, *Geological Society Special Publication 299, 317-339.*

596 Baietto A., P. Perello, P. Cadoppi, and G. Martinotti (2009), Alpine tectonic evolution and
597 thermal water circulations of the Argentera Massif (South-Western Alps), *Swiss J. Geosci.*
598 102, 223-245, doi: 10.1007/s00015-009-1313-5.

599 Bräuer K., H. Kämpf and G. Strauch (2009), Earthquake swarms in non-volcanic regions:
600 what fluids have to say, *Geophys. Res. Lett.*, 36, L17309, doi:10.1029/2009GL039615.

601 Cappa F., J. Rutqvist, and K. Yamamoto (2009), Modeling crustal deformation and rupture
602 processes related to upwelling of deep CO_2-rich fluids during the 1965-1967 Matsushiro
603 earthquake swarm in Japan, J. Geophys. Res., 114, B10304, doi: 10.1029/2009JB006398.

604 Chiodini G., F. Frondini, C. Cardellini, F. Parello, and L. Peruzzi (2000), Rate of diffuse
605 carbon dioxide Earth degassing estimated from carbon balance of regional aquifers: The case
606 central Apennine, Italy, *J. Geophys. Res.*, 105, B4, 8423-8434.

607 Cornet F.H., J. Helm, H. Poitrenaud, and A. Etchecopar (1997), Seismic and aseismic slips
608 induced by large-scale fluid injections, Pure Appl. Geophys. 150, 563-583.

609 Davison A.C., 2003, Statistical models, *Cambridge University Press*, 726p.

610 Dieterich J.H. (1994), A constitutive law for rate of earthquake production and its application
611 to earthquake clustering, *J. Geophys. Res.*, 99 (B2), 2601-2618.
612 Dieterich J.H., V. Cayol, and P. Okubo (2000), The use of earthquakes rate changes as a stress
613 meter at Kilauea volcano, *Nature*, 408, 457-460.
614 Farrell J., Husen S., and Smith R.B. (2009), Earthquake swarm and b-value characterization
615 of the Yellowstone volcano-tectonic system, *J. Volc. Geotherm. Res.*, In Press.
616 Fehler M., L. House, and H. Kaieda (1987), Determining planes along which earthquakes
617 occur: method and application to earthquakes accompanying hydraulic fracturing, Journal of
618 Geophysical Research, 92, B9, pp. 9407-9414.
619 Ferhat G., K.L. Feigl, J.-F. Ritz, and A. Souriau (1998), Geodetic measurement of tectonic
620 deformation in the southern Alps and Provence, France, 1947-1994, Earth Planet. Sci. Lett.,
621 159, 35-46.
622 Fréchet J., and N. Pavoni (1979), Etude de la sismicité de la zone briançonnaise entre Pelvoux
623 et Argentera (Alpes Occidentales) à l'aide d'un réseau de stations portables, *Eclogae geol.*
624 *Helv.*, 72, 3, 763-779.
625 Guyoton, F., J. Fréchet, and F. Thouvenot (1990), La crise sismique de janvier 1989 en
626 Haute-Ubaye (Alpes de Haute Provence, France): étude fine de la sismicité par le nouveau
627 réseau SISMALP, C. R. Acad. Sci. Paris, 311, II, 985-991.
628 Gutenberg, B., and C.F. Richter (1956), Earthquake magnitude, intensity, energy, and
629 acceleration, *Bull. Seismol. Soc. Am.,* 46, 105-145.
630 Hainzl, S., and Y. Ogata (2005), Detecting fluid signals in seismicity data through statistical
631 earthquake modeling, *J. Geophys. Res,* 110, B05S07, doi:10.1029/2004JB003247.

632 Hainzl, S., F. Scherbaum, and C. Beauval (2006), Estimating background activity based on
633 interevent-time distribution, *Bull. Seismol. Soc. Am.*, 96, 1, pp. 313-320.
634 Hainzl, S., and T. Kraft (2006), Analysis of complex seismicity pattern generated by fluid
635 diffusion and aftershock triggering, *4th International Workshop on Statistical Seismology*
636 *(STATSEI4), Japan, 9-13 January.*
637 Helmstetter, A., D. Sornette, and J.-R. Grasso (2003a), Mainshocks are aftershocks of
638 conditional foreshocks: How do foreshock statistical properties emerge from aftershock laws,
639 *J. Geophys. Res*., 108, 2046, doi:10.1029/2002JB001991.
640 Helmstetter A., G. Ouillon, and D. Sornette (2003b), Are aftershocks of large Californian
641 earthquakes diffusing?, *J. Geophys. Res.*, 108, B10, 2483, doi:10.1029/2003JB002503.
642 Hill D.P. (1977), A model for earthquake swarm*, J. Geophys. Res.* 82, 8, 1347-1352.
643 Hill D.P. and S. Prejean (2005), Magmatic unrest beneath Mammoth Mountain, California, *J.*
644 *Volc. Geotherm. Res.*, 146, 257-283.
645 Horálek J., and T. Fischer (2008), Role of crustal fluids in triggering the West
646 Bohemia/Vogtland earthquake swarms: just what we know (a review), *Stud. Geophys. Geod.*,
647 52, 455-478.
648 Huc M., and I.G. Main (2003), Anomalous stress diffusion in earthquake triggering:
649 Correlation length, time dependence, and directionality, *J. Geophys. Res.*, 108, B7, 2324,
650 doi:10.1029/2001JB001645.
651 Jenatton, L., R. Guiguet, F., Thouvenot, and N. Daix (2007), The 16,000-event 2003-2004
652 earthquake swarm in Ubaye (French Alps), *J. Geophys. Res., 112, B11304,*
653 doi:10.1029/2006JB004878.

654 Kagan, Y.Y., and L. Knopoff (1987), Statistical short-term earthquake prediction, *Science*
655 236, 4808, 1563-1567.

656 Llenos, A.L., J.J. McGuire, and Y. Ogata (2009), Modeling seismic swarms triggered by
657 aseismic transients, *Earth Planetary Sci. Lett*., 281, 59-69.

658 Linker M.F., and Dieterich J.H (1992), Effect of variable normal stress on rock friction:
659 observations and constitutive equations, *J. Geophys. Res.*, 97, 4923-4940.

660 Lohman, R.B., and J.J. McGuire (2007), Earthquake swarms driven by aseismic creep in the
661 Salton Trough, California*, J. Geophys. Res.*, 112, B04405, doi:10.1029/2006JB004596.

662 Marsan D., C.J. Bean, S. Steacy, and J. McCloskey (1999), Spatio-temporal analysis of stress
663 diffusion in a mining-induced seismicity system, *Geophys. Res. Lett.*, 26, 24,3697-3700.

664 Marsan D., C.J. Bean, S. Steacy, and J. McCloskey (2000), Observation of diffusion
665 processes in earthquake populations and implications for the predictability of seismicity
666 systems, *J. Geophys. Res.*, 105, B12, 28081-28094.

667 Marsan D., and O. Lengline (2008), Extending earthquakes' reach through cascading,
668 Science, 319, 5866, pp. 1076-1079, doi:10.1126/science.1148783.

669 Matsu'ura R.S., and I. Karakama (2005), A point-process analysis of the Matsushiro
670 earthquake swarm sequence: the effect of water on earthquake occurrence, *Pure Appl.*
671 *Geophys.*, 162, 1319-1345, doi: 10.1007/s00024-005-2672-0.

672 Miller S.A., C. Collettini, L. Chiaraluce, M. Cocco, M. Barchi, and B.J.P. Kaus (2004),
673 Afteshocks driven by a high-pressure CO_2 source at depth, *Nature* 427, 724-727, doi:
674 10.1038/nature02251.

675 Noir J., E. Jacques, S. Békri, P.M. Adler, P. Tapponnier, and G.C.P. King (1997), Fluid flow
676 triggered migration of events in the 1989 Dobi earthquake sequence of Central Afar, *Geophys.*
677 *Res. Lett.*, 24, 18, 2335-2338.
678 Nur, A., and J. R. Booker (1972), Aftershocks caused by pore fluid flow ?, *Science*, 175,
679 4024, pp. 885-887, doi:10.1126/science.175.4025.885.
680 Ogata Y. (1988), Statistical models for earthquake occurrences and residual analysis for point
681 processes, *J. Am. Stat. Assoc.*, 83, pp. 9-27.
682 Ogata Y. (1992), Detection of precursory relative quiescence before great earthquakes
683 through a statistical model, *J. Geophys. Res.* 97, 19845-19871.
684 Savage J.C., and R.S. Cockerham (1984), Earthquake swarm in Long Valley Caldera,
685 California, January 1983: Evidence for dike inflation, *J. Geophys. Res.*, 89, B10, 8315-8324.
686 Shapiro S.A., E. Huenges, and G. Borm (1997), Estimating the crust permeability from fluid-
687 injection-induced seismic emission at the KTB site, *Geophys. J. Int.*, 131, F15-F18.
688 Shapiro S. A., J. Kummerow, C. Dinske, G. Asch, E. Rothert, J. Erzinger, H.-J. Kümpel, and
689 R. Kind (2006a), Fluid induced seismicity guided by a continental fault: injection experiment
690 of 2004/2005 at the German Deep Drilling Site (KTB), *Geophys. Res. Lett.*, 33, L14312,
691 doi:10.1029/2006GL026365.
692 Shapiro, S. A., C. Dinske, and E. Rothert (2006b), Hydraulic-fracturing controlled dynamics
693 of microseismic clouds, *Geophys. Res. Lett.*, 33, L14312, doi:10.1029/2006GL026365.
694 Shapiro S.A. and C. Dinske (2009), Scaling of seismicity induced by nonlinear fluid-rock
695 interaction, *J. Geophys. Res.*, 114, B09307, doi:10.1029/2008JB006145.
696 Sue, C. (1998), Dynamique actuelle et récente des Alpes occidentals internes –Approches
697 structurale et sismologique, *Ph.D. Thesis*, Univ. Joseph Fourier, Grenoble, France.

698 Thouvenot F., J. Fréchet, F. Guyoton, R. Guiguet, and L. Jenatton (1990), Sismalp: an
699 automatic phone-interrogated seismic network for the western Alps, *Cahiers du Centre*
700 *Européen de Géodynamique et de Sismologie*, 1, 1-10.
701 Thouvenot F. and J. Fréchet (2006), Seismicity along the northwestern edge of the Adria
702 microplate, in *The Adria Microplate: GPS Geodesy, Tectonics, and Hazards*, edited by N.
703 Pinter et al., pp. 100–120, Springer, Dordrecht, Netherlands.
704 Toda S. and Stein R. (2002), Evidence for the AD 2000 Izu islands earthquake swarm that
705 stressing rate governs seismicity, *Nature*, 419, 58-61.
706 Tsuneishi Y. and K. Nakamura (1970), Faulting associated with the Matsushiro swarm
707 earthquakes, *Bull. Earthq. Res. Ins.*, 48, 29-51.
708 Ukawa M., and H. Tsukahara (1996), Earthquake swarms and dike intrusions off the east
709 coast of Izu Peninsula, central Japan, *Tectonophysics*, 253, 285-303.
710 Vlahos L., H. Isliker, Y. Kominis, and K. Hizanidis (2008), Normal and anomalous diffusion:
711 a tutorial, *arXiv*:0805.0419v1.
712 Waldhauser, F., and W. L. Ellsworth (2000), A double-difference earthquake location
713 algorithm: Method and application to the Northern Hayward Fault, California, *Bull. Seismol.*
714 *Soc. Am.*, 90, 1353-1368.
715 Weinlich F.H., K. Bräuer, H. Kämpf, G. Strauch, J. Tesär, and S.M. Weise (1999), An active
716 subcontinental mantle volatile system in the Western Eger rift, Central Europe: Gas flux,
717 isotopic (He, C, and N) and compositional fingerprints, *Geochem. Cosmo. Acta*, 63, 21, 3653-
718 3671.

719 Yamashita T. (1999), Pore creation due to fault slip in a fluid-permeated fault zone and its
720 effect on seismicity: generation mechanism of earthquake swarm, *Pure Appl. Geophys.*, 155,
721 625-647.
722 Zoback M.D., and H.-P. Harjes (1997), Injection-induced earthquakes and crustal stress at 9
723 km depth at the KTB deep drilling site, Germany, *J. Geophys. Res.*, 102, B8, 18,477-18,491.
724
725
726

727

Window starting time (days)	0	130.7	174	350.8	458.8	614.9
Window ending time (days)	130.7	174	350.8	458.8	614.9	730
$\lambda_0(t)$ (event/day) *Hainzl et al (2006)*'s method	**1.06**	**2.52**	**4.99**	**1.78**	**0.65**	**0.24**
$\lambda_0(t)$ (event/day) Alternative 1: Joint inversion	0.92	3.04	3.79	0.76	0.41	0.27
$\lambda_0(t)$ (event/day) Alternative 2: Background reconstruction method	0.66	2.93	2.84	0.35	0.21	0.03

728

729 Table 1: Limits of optimal time windows and amplitude of the background rate. We here
730 present background rate estimates obtained from three different algorithms. Best adjustments
731 are obtained using *Hainzl et al. (2006)*'s method. Two alternative techniques were tested. The
732 first one inverts jointly ETAS epidemic parameters and background values. The second
733 technique reconstructs the background rate from the difference between the observed rate of
734 event and the rate of triggered events (obtained from the ETAS triggering kernel and A, α, c,
735 and p estimates). The differences between the background estimates for the alternative
736 techniques 1 and 2 may partly be due to the smoothing used for the background reconstruction
737 technique (alternative 2), and to the use of different sets of ETAS parameters A, α, c, and p.
738 See section 4-2.

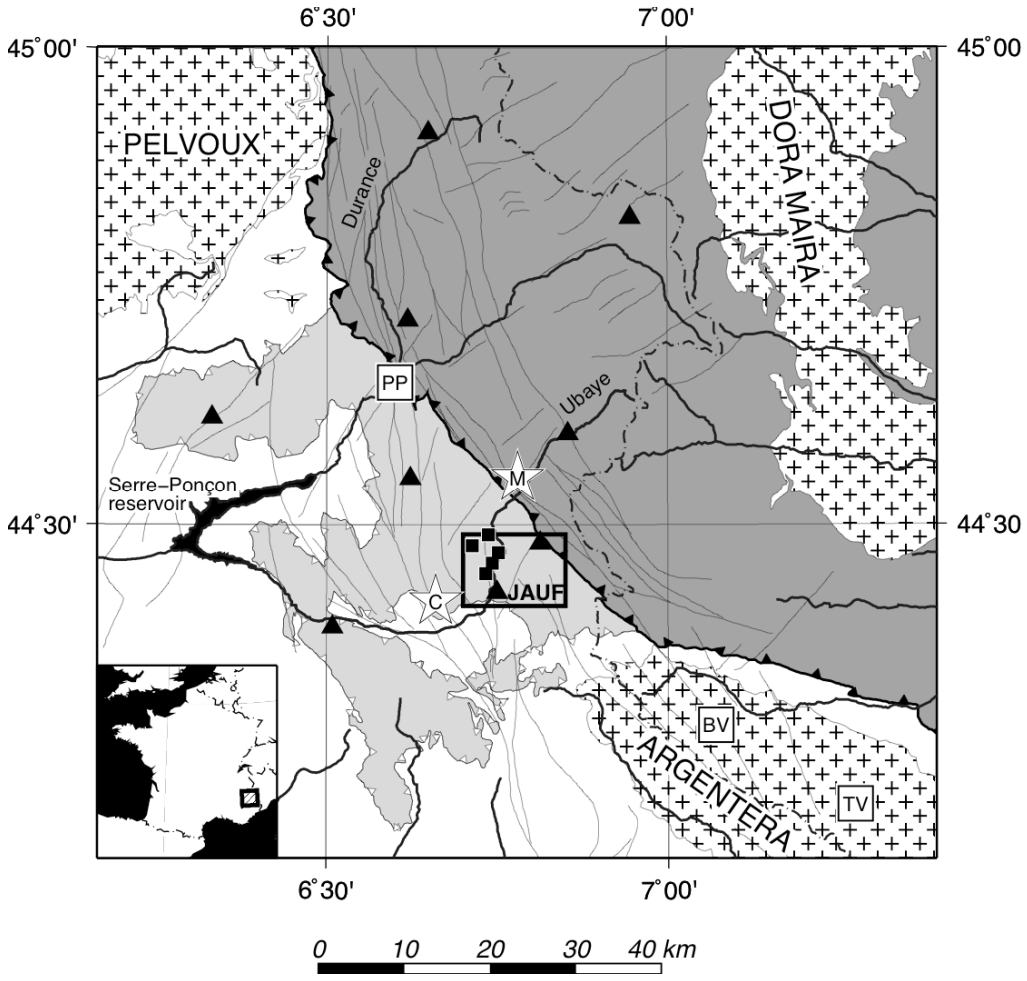

739

740 **Figure 1:** Map of the Southwestern Alps with main geological features. Crossed areas stand
741 for the Pelvoux, Argentera and Dora Maira crystalline massifs. The lightly shaded area is the
742 Embrunnais-Ubaye nappes. The dark gray area is the Peninnic domain. Fault traces after *Sue*
743 *(1998)*. Stars correspond to macro-seismic (M) and computed (C) epicenters of the 1959 M
744 5.5 St-Paul-sur-Ubaye damaging earthquake. Black triangles are permanents seismological
745 stations from the Sismalp network, and black squares stand for temporary seismological
746 stations deployed in the area from September 2003. White squares are hot springs. PP: Plan de
747 Phasy; BV: Bagni di Vinadio; TV: Terme di Valdieri. The dash-dotted line is the French-
748 Italian border. The study area is delimitated by the box in the center of the map. Modified
749 from *Jenatton et al., 2007*.

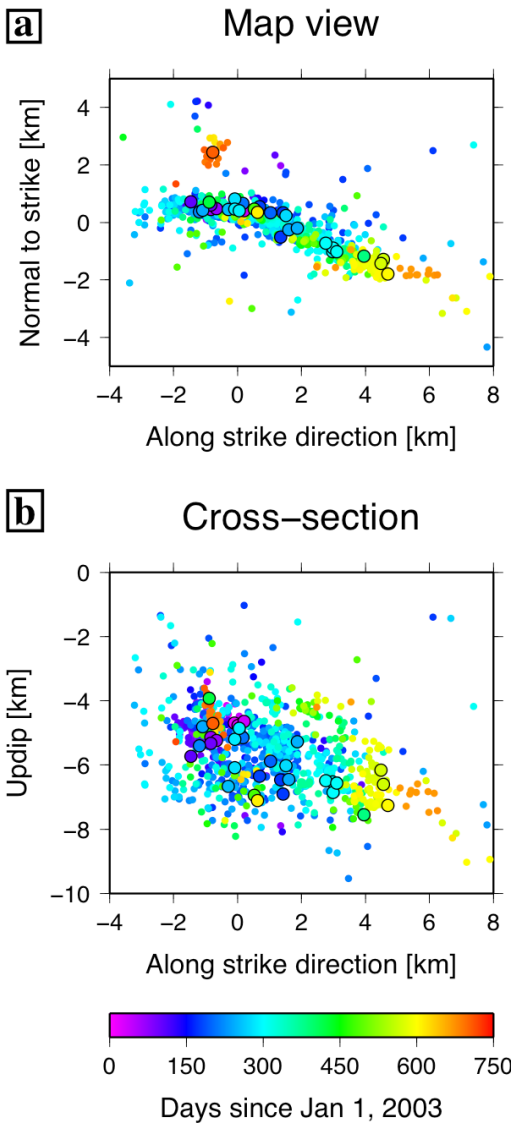

750

751 **Figure 2:** Map of the Ubaye 2003-2004 seismic swarm. The panels present a relocation of
752 974 seismic events a) in map view and b) in cross-section. Coordinates are projected on a
753 planar orientation striking N130E, and dipping 80°W. Origins of coordinate axes correspond
754 to the surface projection of the swarm centroid (with geographical coordinates 44°27.2N,
755 6°45E). Depth is expressed relatively to the sea level. Small dots stand for events with
756 magnitude less than 2, and large dots represent earthquakes with magnitude larger than, or
757 equal to 2. The color-scale highlights the date of each earthquake from January 2003
758 (magenta) to December 2004 (red).

759

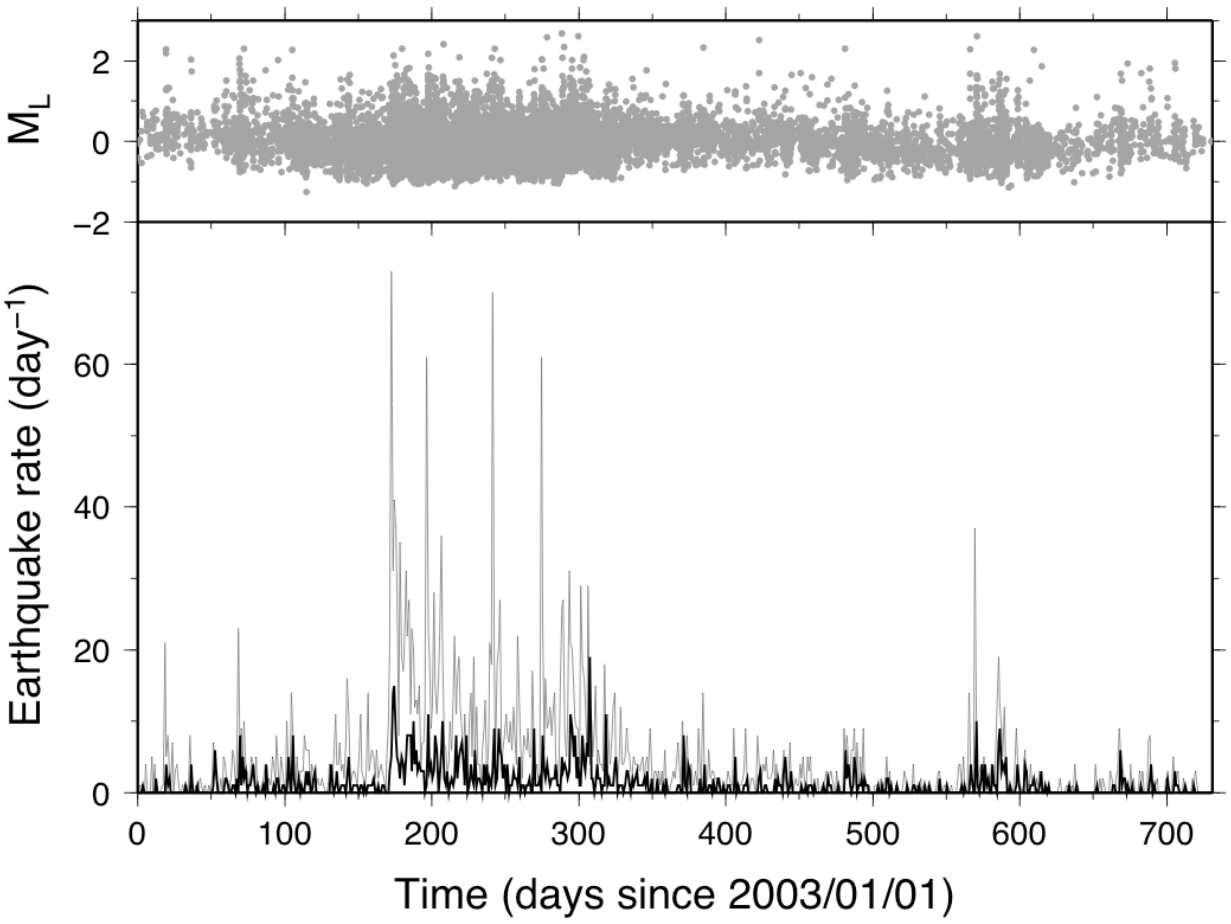

760

761 **Figure 3: (Top)** Timeseries and magnitudes of the 16,147 events recorded at station JAUF
762 between Jan 1st, 2003 (day 0) and Dec 31st, 2004 (day 730). **(Bottom)** Rate of $M_L \geq 0.2$
763 earthquakes detected at station JAUF (grey curve) and of $M_L \geq 1$ earthquakes relocated in this
764 study (black curve, see also Figure 2).

765

766

767

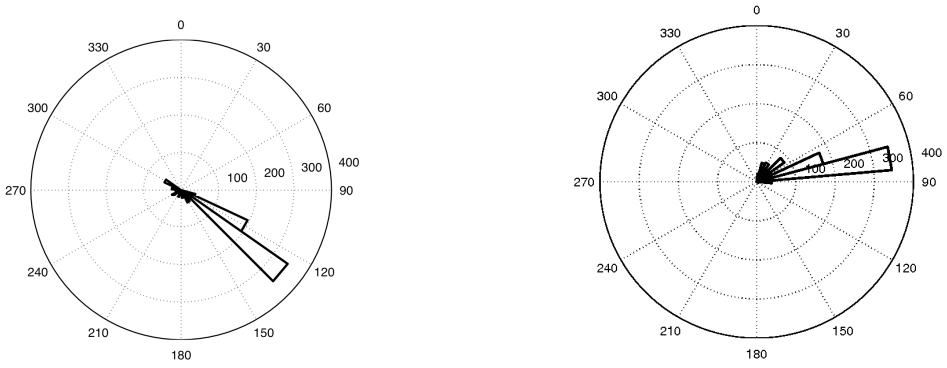

768

769

770

771 **Figure 4:** Distributions of strike (left) and dip (right) angles for planes associated with seismic
772 events of the relocated catalogue. Plane orientations were estimated for each possible set of 3
773 earthquakes using the method of *Fehler et al. (1987)*. Sector length indicates the number of
774 earthquakes associated with each plane orientation. On the left diagram, sector direction
775 indicates the azimuth of planes, with 0° and 90° standing respectively for the North and the
776 East directions. Bins are 10° wide. A clear preeminence exists for events occurring along
777 planes striking N130°E and dipping 80°W.

778

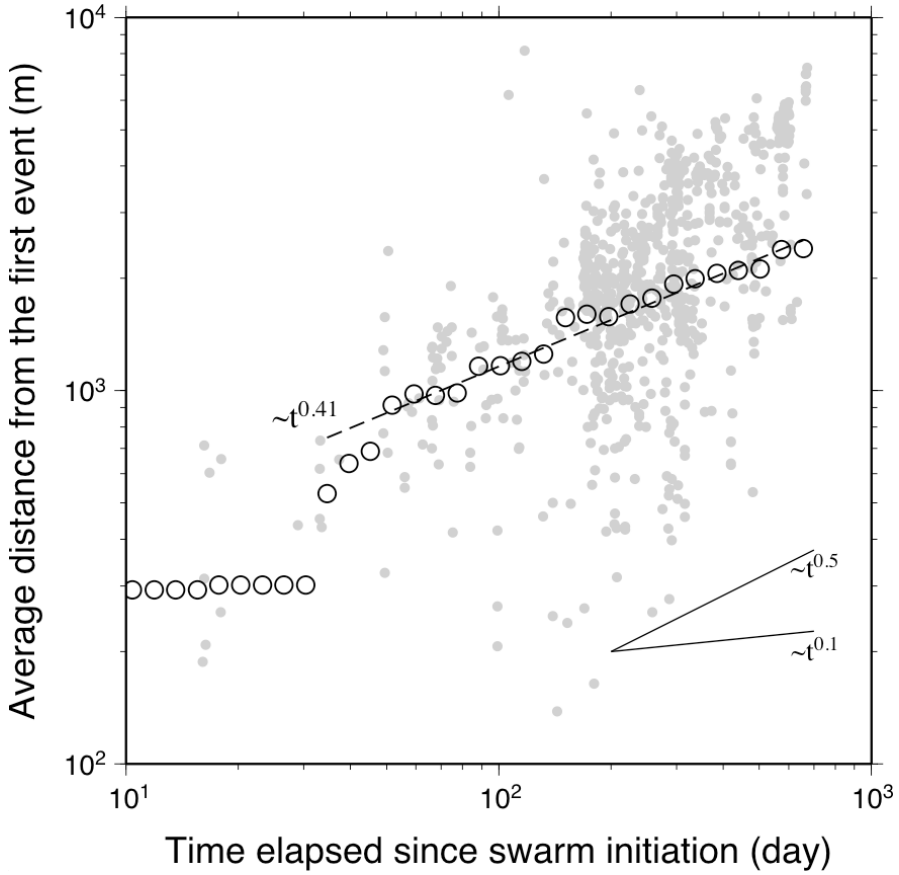

779

780

781 **Figure 5:** Characteristic size R of the main swarm cluster as a function of time. For a given
782 time t, R is measured as the average distance between all swarm events that occurred at time
783 $t_i<t$ and the first earthquake of the sequence. After ~30 days of relative stability, this average
784 distance increases as $R \sim t^H$ with $H=0.41 \pm 0.06$. For the sake of comparison, we have
785 represented in the lower right corner slopes that should be expected for a normal diffusive
786 process ($H=0.5$) and for a typical sub-diffusive process expected during aftershock sequences
787 ($H=0.1$). Information on the spreading of the data is given by the grey solid circles, which
788 indicate the distance between every relocated earthquake and the first one of the sequence.

789

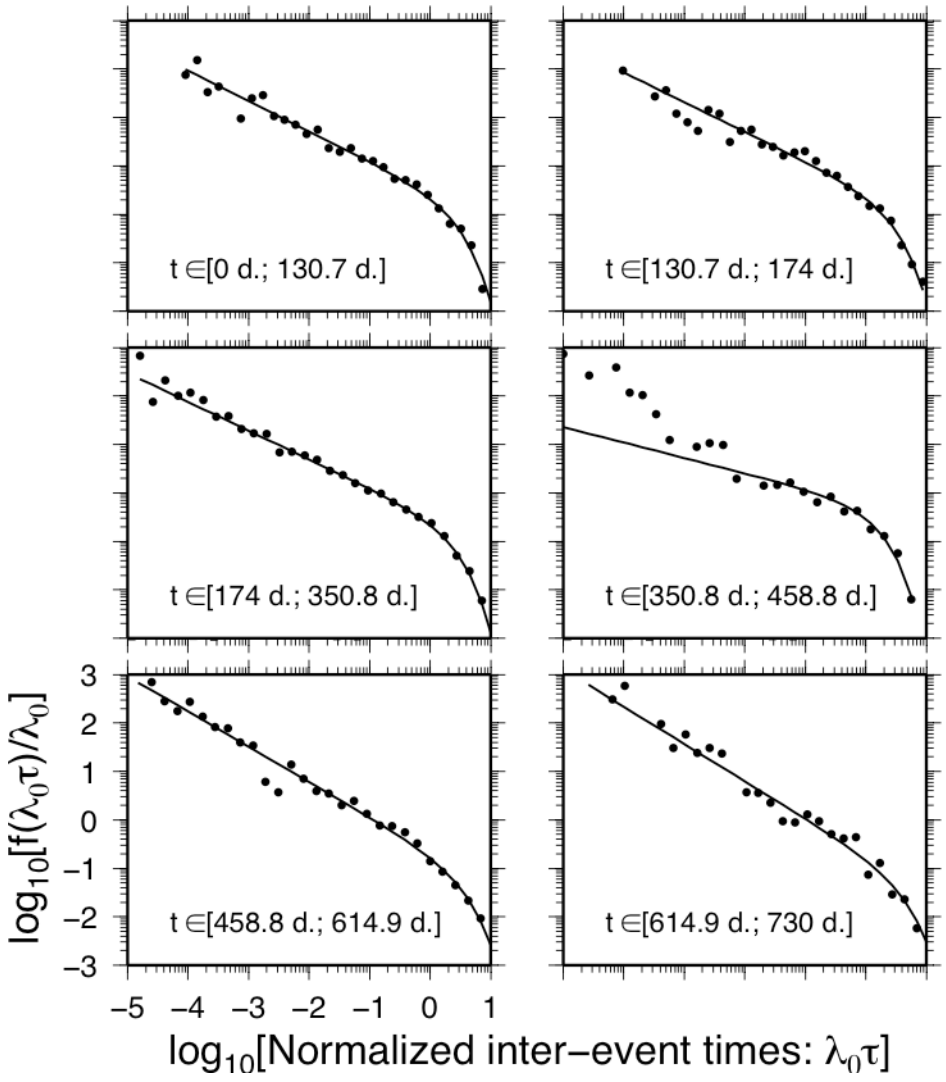

790

791 **Figure 6:** Adjustment of inter-event times distributions (dots) by a Gamma distribution
792 (curve), according to a maximum likelihood method. Each subplot corresponds to the inter-
793 event times distribution for a single time window with a constant background rate $\lambda_0(t)$. Time
794 windows are defined by a change-point analysis, based on significant changes in successive
795 inter-event time distributions (see section 4-1).

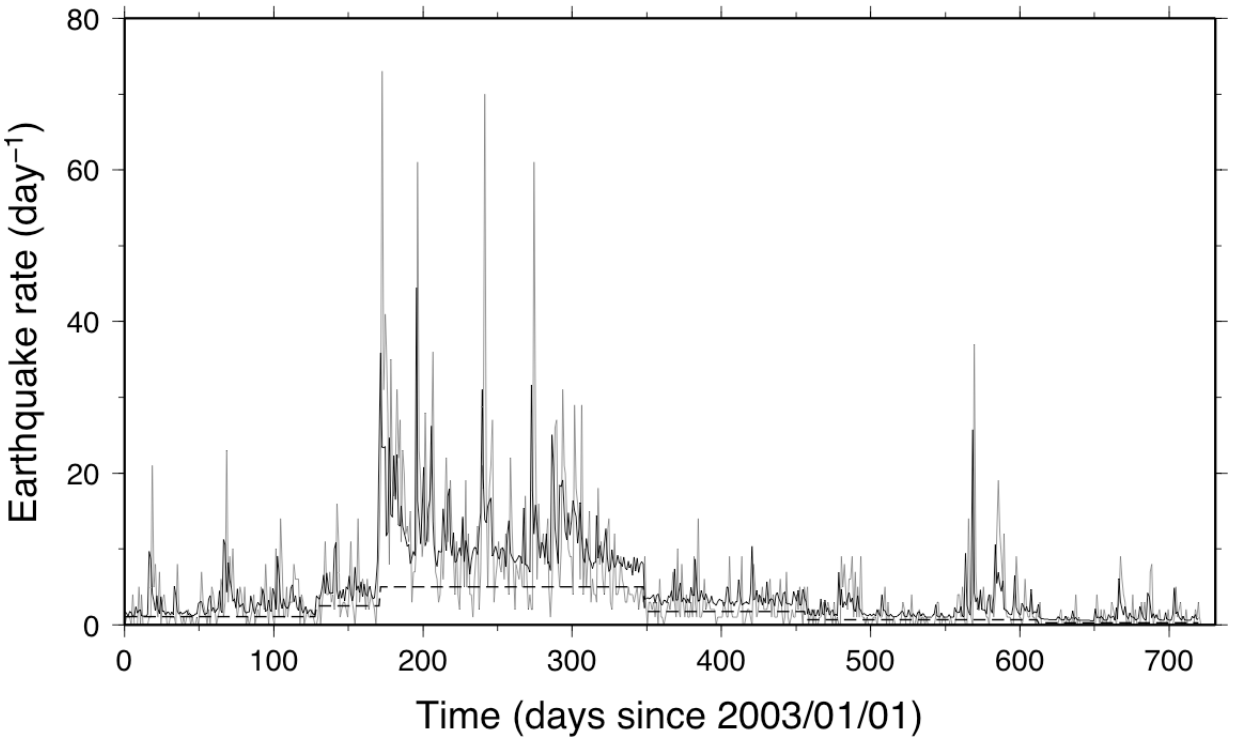

796

797

798 **Figure 7:** Comparison of the Ubaye seismic activity detected at station JAUF (gray curve)
799 with the best non-stationary ETAS model (black curve), see equations (2) and (3). Best
800 epidemic parameter estimates are A=0.0199, α=1.246, c=1.35·10^{-4} day and p=1.065. The
801 stair-step dashed line stands for the non-stationary background contribution λ_0(t) to the
802 seismicity rate. See also Table 1 for a report on the amplitude of λ_0(t) for each time window.
803 This stair-step shape arises from the determination of optimal time windows with a constant
804 background rate λ_0(t), as determined by the change-point method explained in section 4-1.
805 This method is based on inter-event time adjustments presented on Figure 6.

806

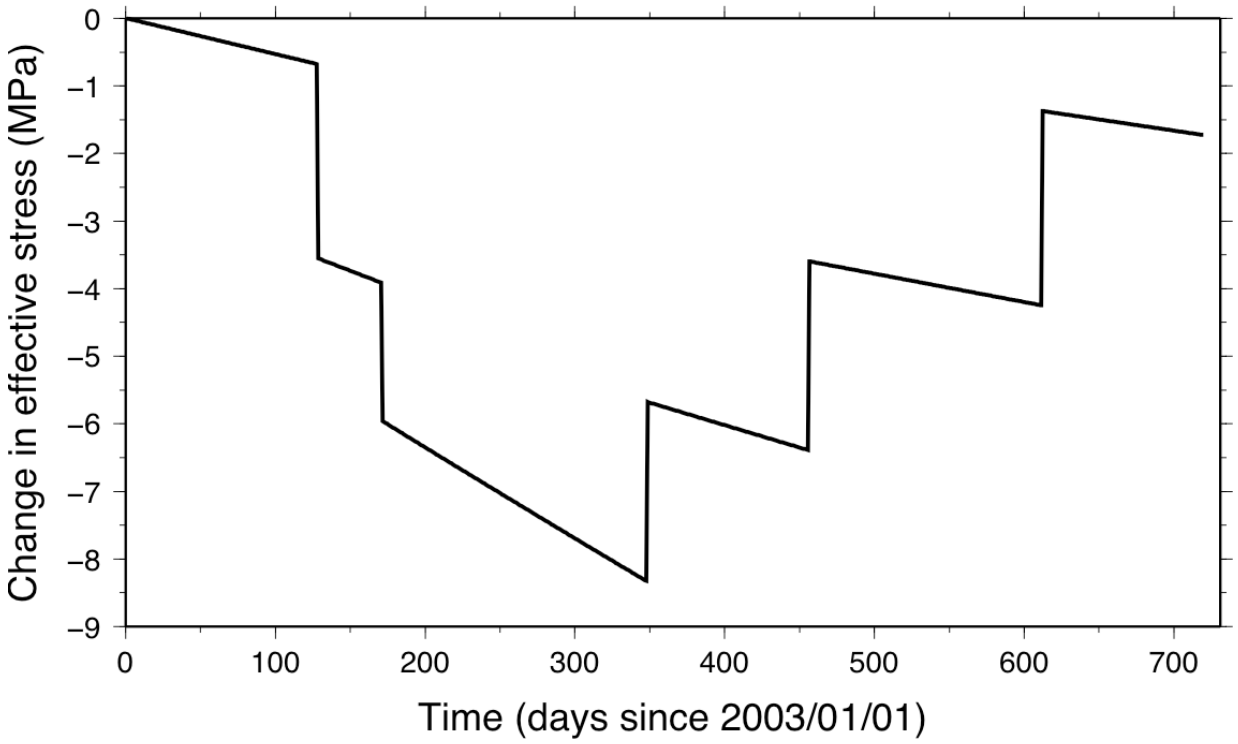

807

808

809 **Figure 8:** Changes in effective stress integrated over the swarm area. These changes are
810 estimated from the rate of background event $\lambda_0(t)$ represented on figure 7, and by use of rate-
811 and-state constitutive laws for earthquake production [*Dieterich, 1994; Dieterich et al., 2000*],
812 see section 5. We supposed that this seismicity rate was triggered by changes in effective
813 stress under a constant shear stressing rate of 2.5×10^{-3} MPa.yr^{-1}. Effective stress is expressed
814 relatively to the steady-state value of 83.4 MPa before the swarm initiation. This value comes
815 from the difference in overburden pressure (with bulk density ρ=2700 kg.m^{-3}) minus the
816 hydrostatic pressure at z=5 km.

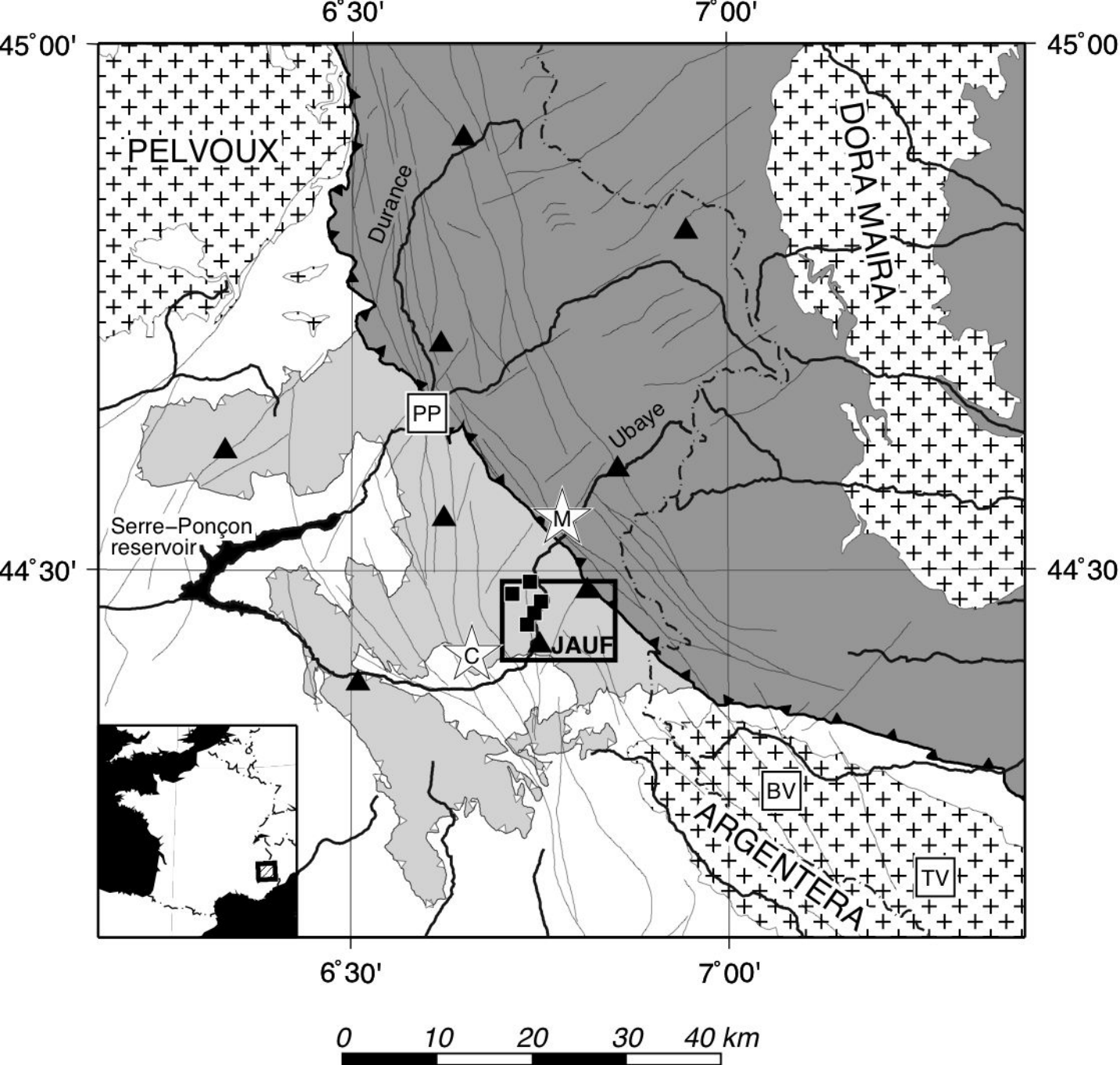
6°30'
7°00'
45°00'
45°00
44°30'
44°30
PELVOUX
Durance
DORA MAIRA
Ubaye
PP
M
Serre–Ponçon
reservoir
JAUF
C
BV
TV
ARGENTERA
0 10 20 30 40 km

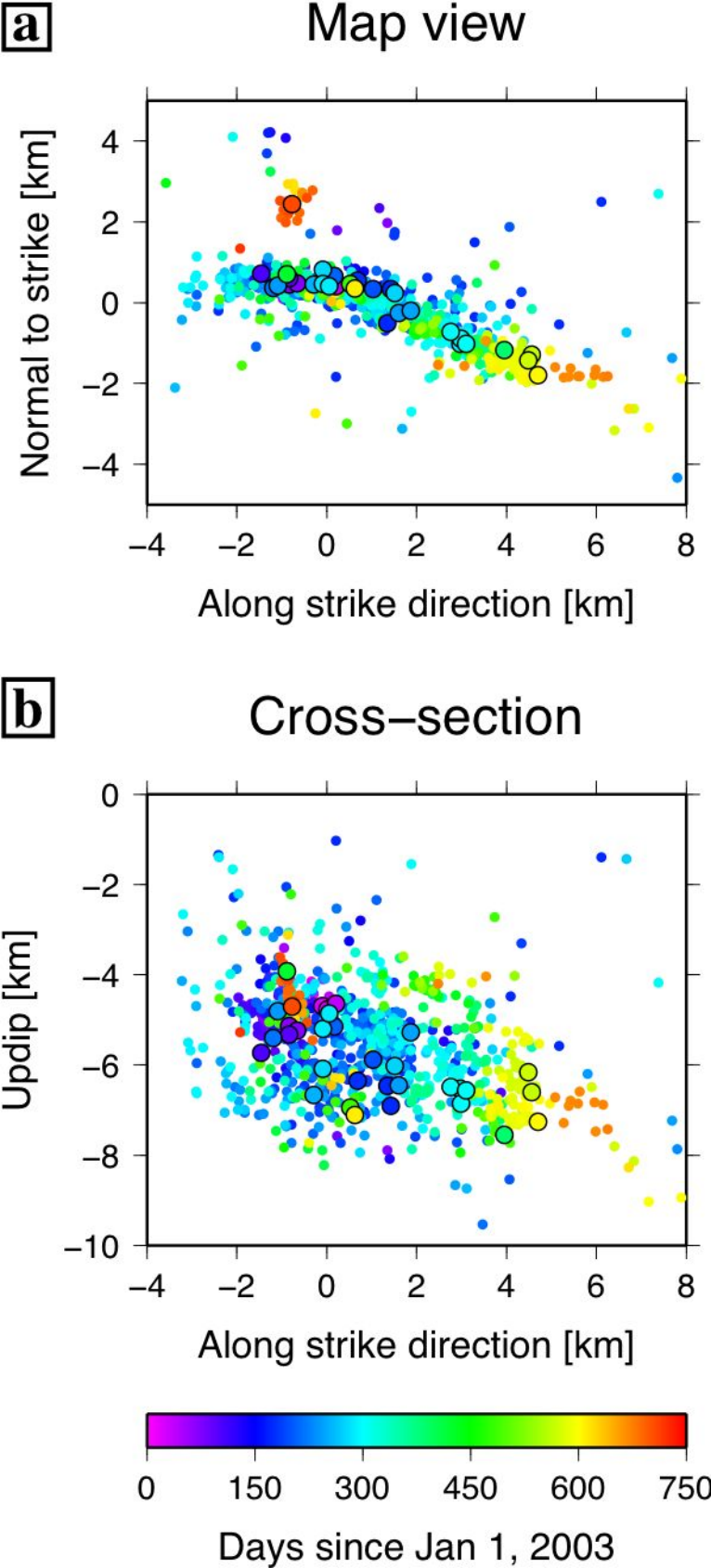
a
Map view
Normal to strike [km]
4
2
0
−2
−4
−4
−2
0
2
4
6
8
Along strike direction [km]
b
Cross−section
Updip [km]
0
−2
−4
−6
−8
−10
−4
−2
0
2
4
6
8
Along strike direction [km]
0
150
300
450
600
750
Days since Jan 1, 2003

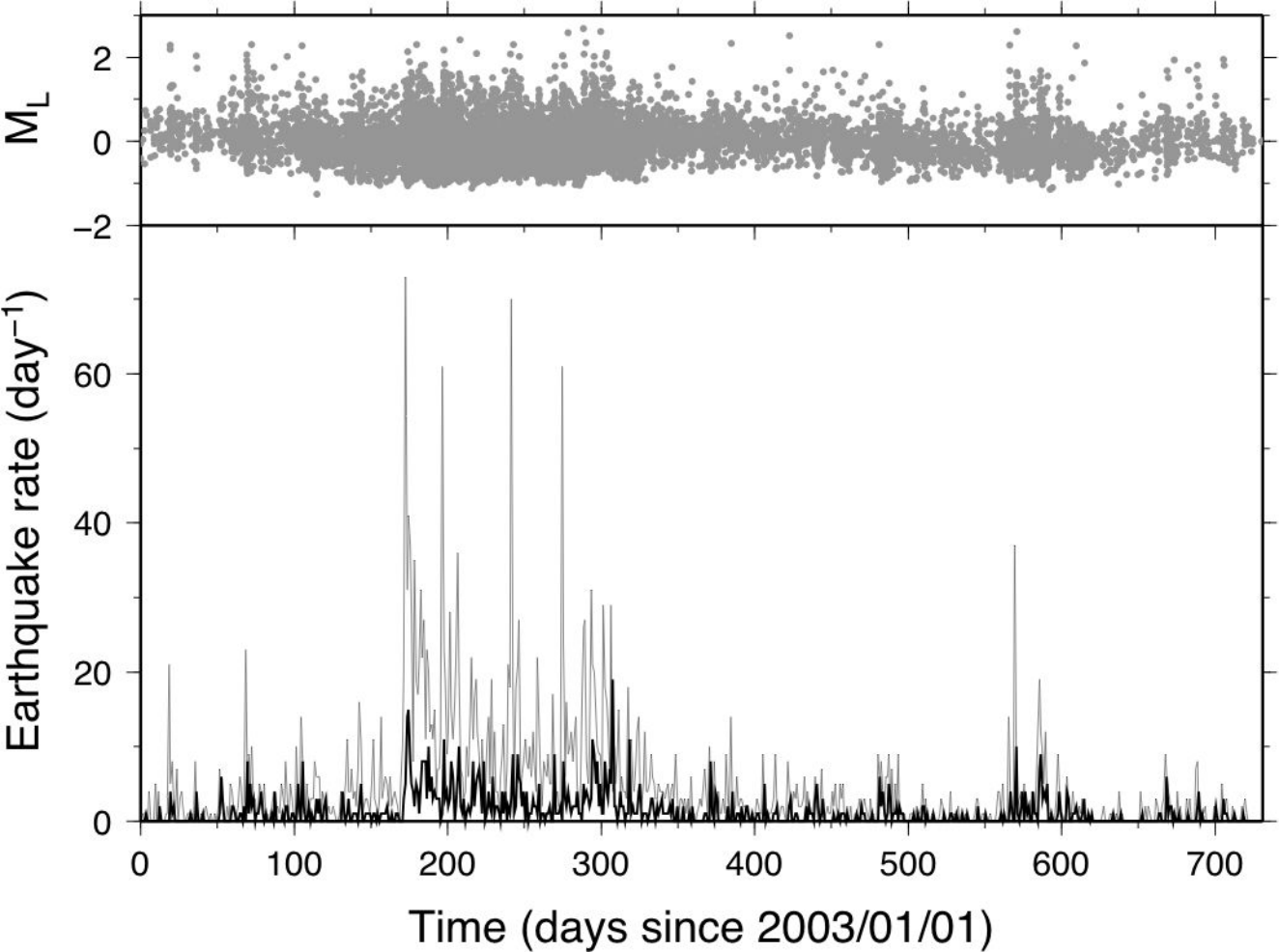
M_L
2
0
−2
Earthquake rate (day^{-1})
60
40
20
0
0
100
200
300
400
500
600
700
Time (days since 2003/01/01)

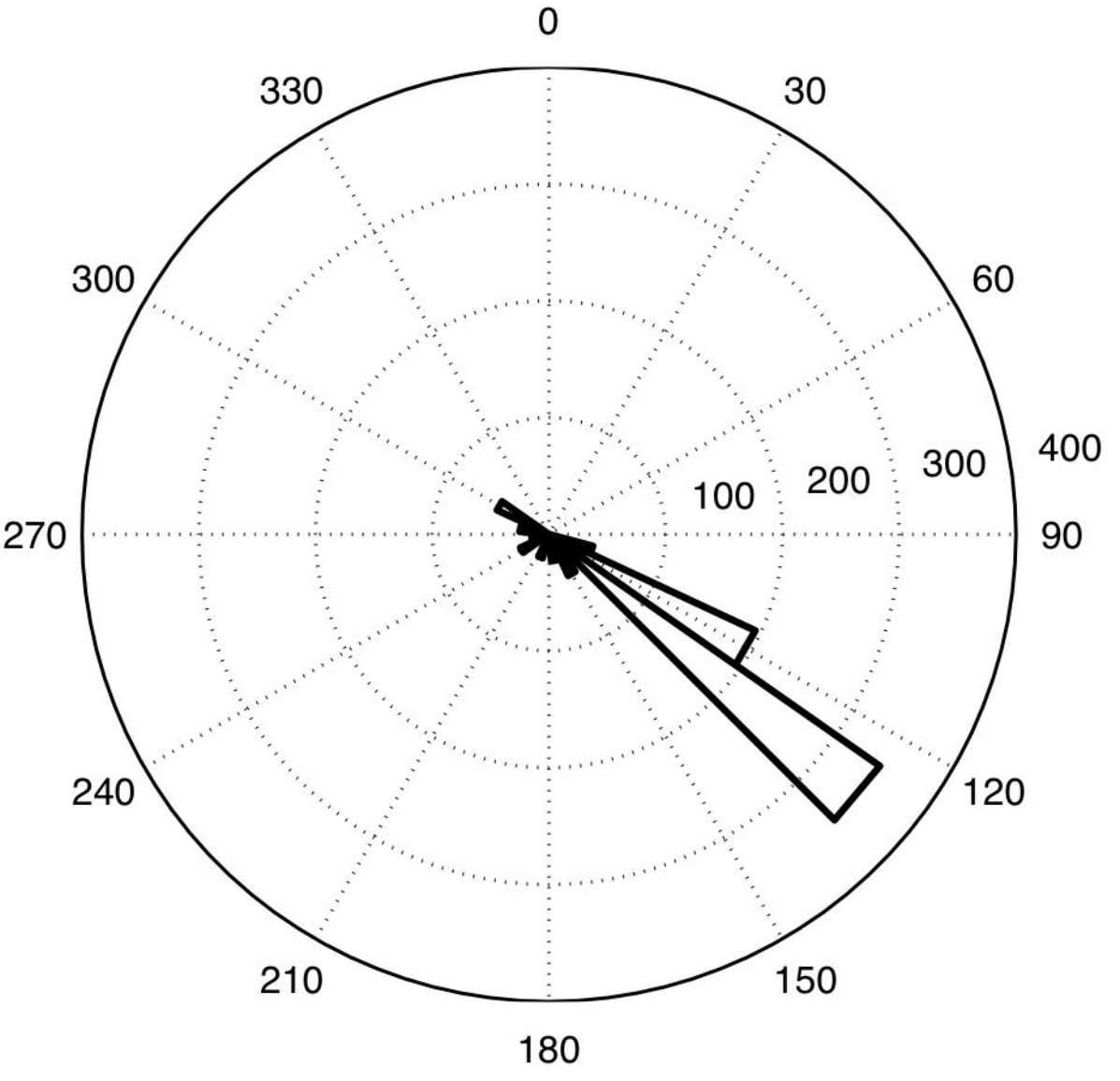
0
30
60
90
120
150
180
210
240
270
300
330
100
200
300
400

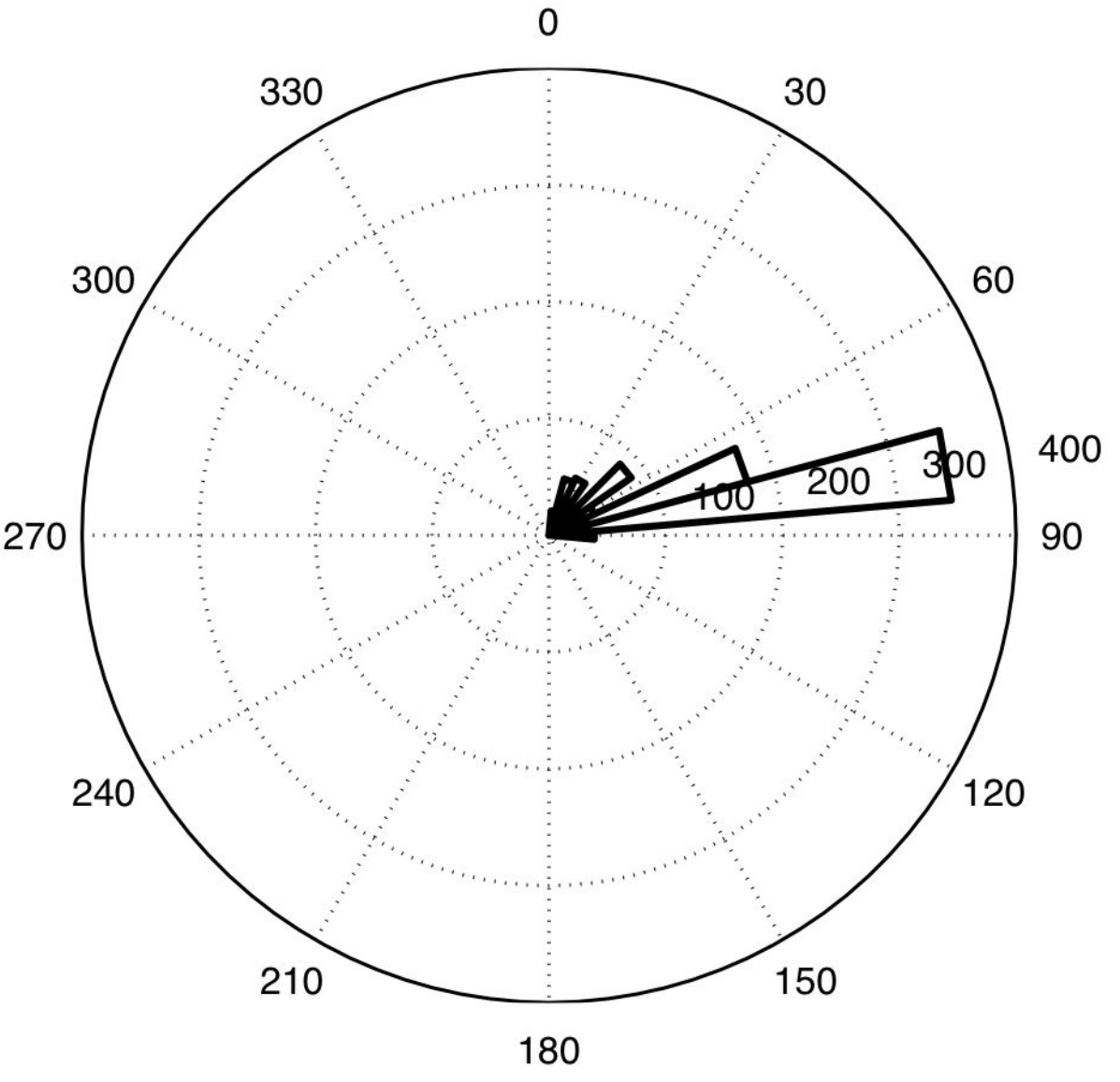
0
30
60
90
120
150
180
210
240
270
300
330
100
200
300
400

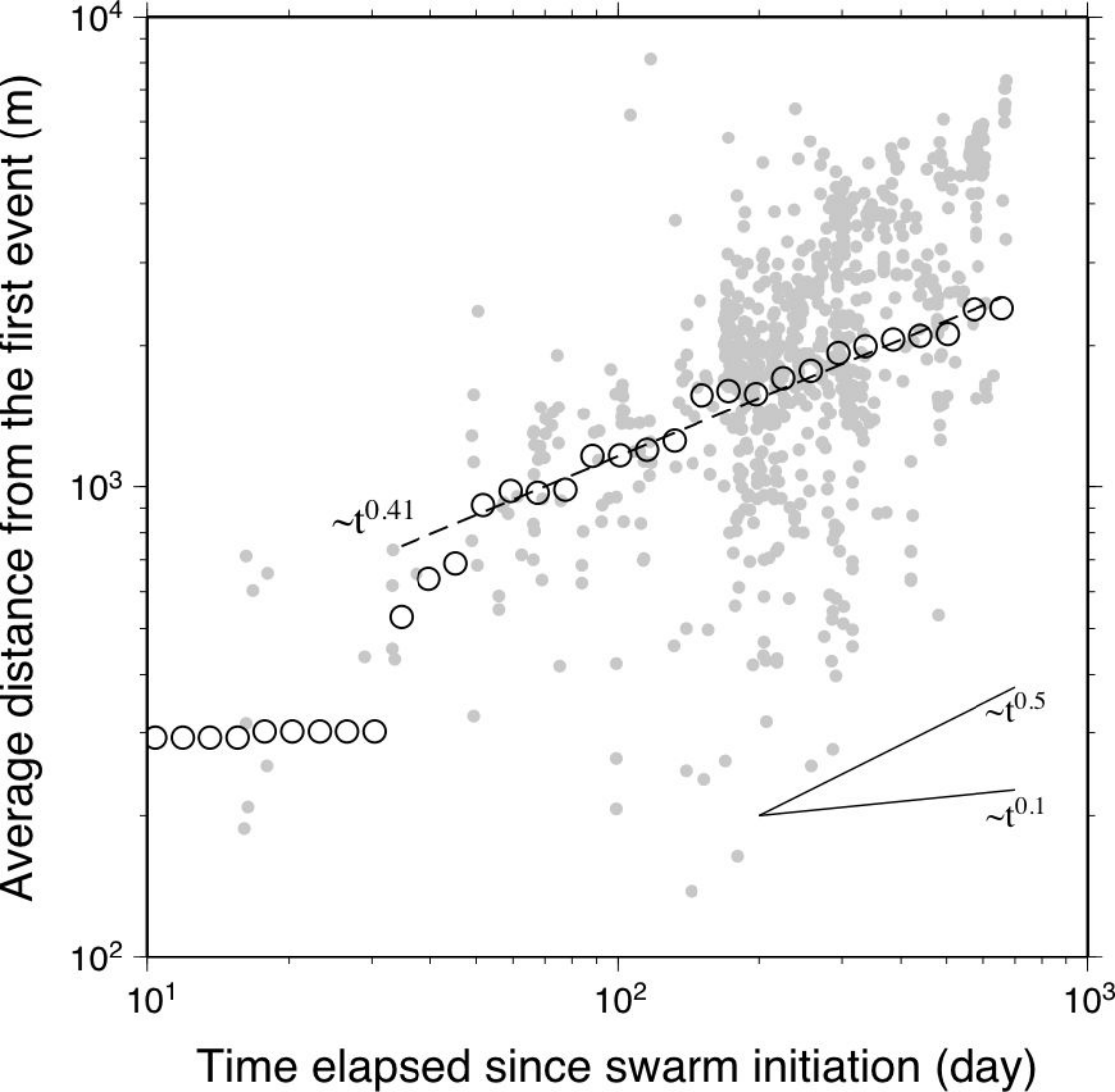
Average distance from the first event (m)
Time elapsed since swarm initiation (day)
10^4
10^3
10^2
10^1
10^2
10^3
~t^0.41
~t^0.5
~t^0.1

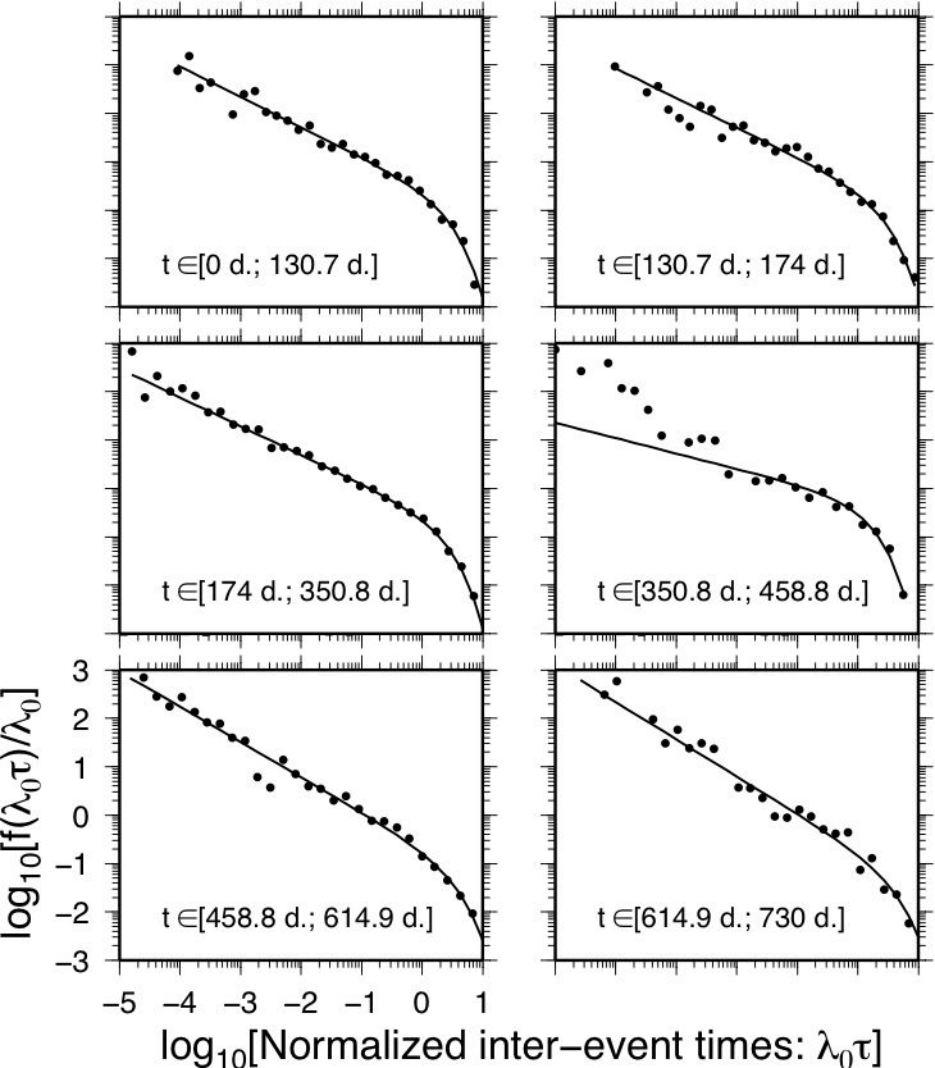
t ∈[0 d.; 130.7 d.]
t ∈[130.7 d.; 174 d.]
t ∈[174 d.; 350.8 d.]
t ∈[350.8 d.; 458.8 d.]
t ∈[458.8 d.; 614.9 d.]
t ∈[614.9 d.; 730 d.]
log10[f(λ0τ)/λ0]
log10[Normalized inter−event times: λ0τ]
3
2
1
0
−1
−2
−3
−5
−4
−3
−2
−1
0
1

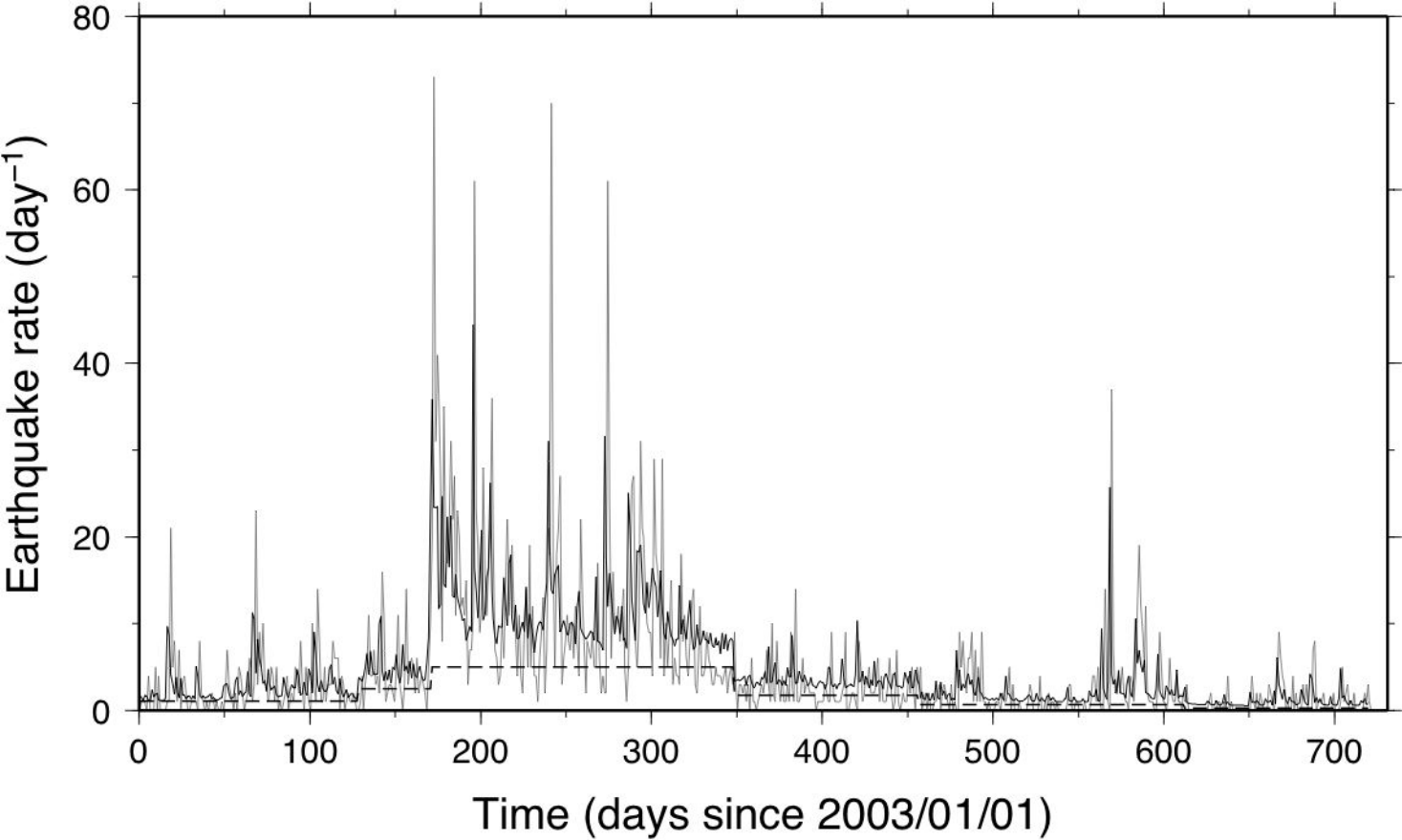
80
60
40
20
0
Earthquake rate (day^{-1})
0
100
200
300
400
500
600
700
Time (days since 2003/01/01)

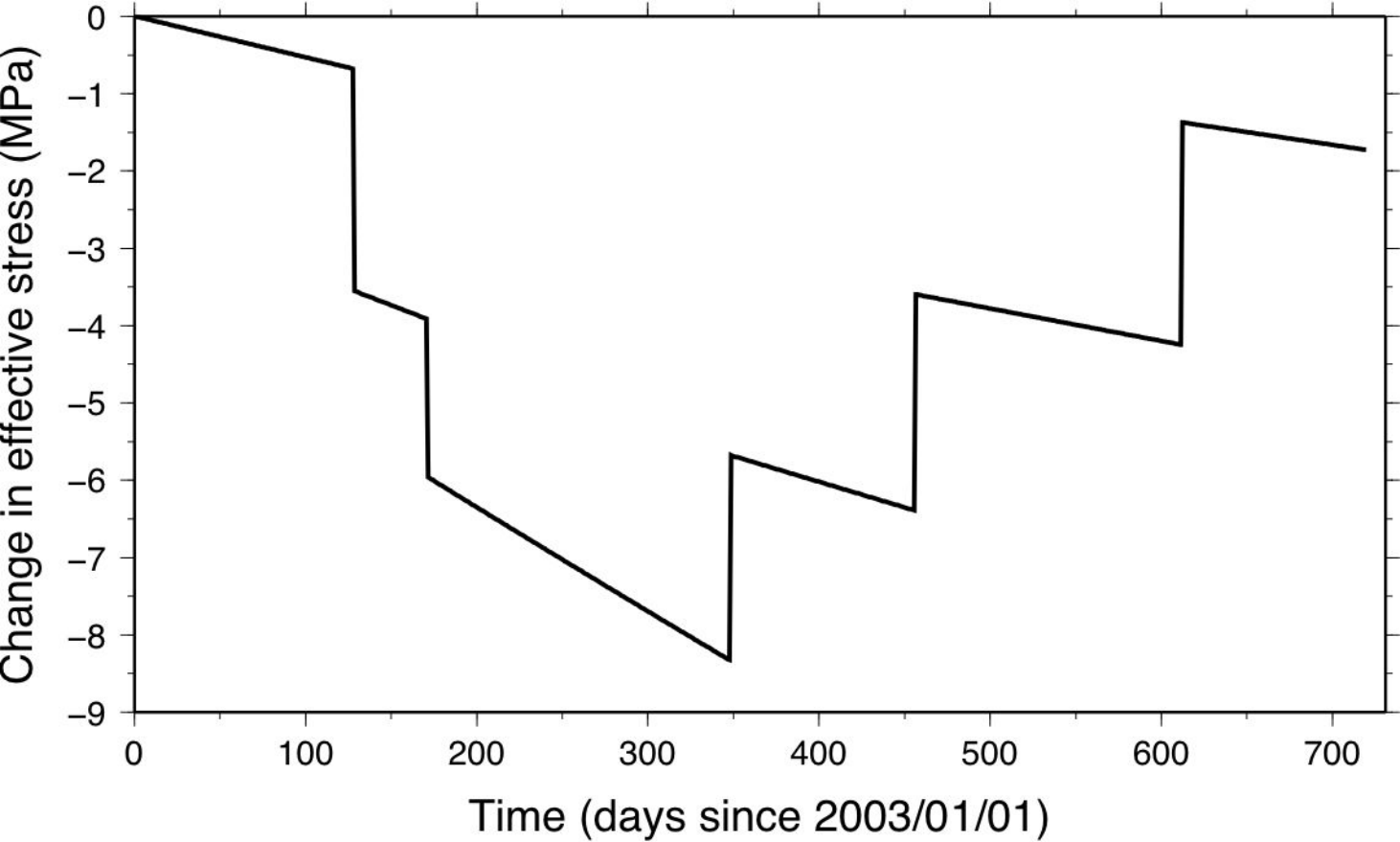
Change in effective stress (MPa)
0
−1
−2
−3
−4
−5
−6
−7
−8
−9
0
100
200
300
400
500
600
700
Time (days since 2003/01/01)